Understanding historical and projected compound change on the Northwest Atlantic shelf

Siedlecki, S.A.[1], Soares, F.[1], Chen, Z.[1], Curchitser, E.[2], Nguyen, H.[1], Meseck, S.L.[3], Alexander, M.A.[4], Shin, S.[4], Matassa, C.M.[1], & Berger, H.[1]

[1] Department of Marine Sciences, University of Connecticut, Groton, U.S.A

[2] Rutgers University, New Brunswick, NJ, U.S.A.

[3] NOAA, Northeast Fisheries Science Center (NEFSC), U.S.A.

[4] NOAA, Physical Sciences Laboratory (PSL), Boulder, CO, U.S.A.

Keywords: Ocean acidification, Northwest Atlantic Shelf, Biogeochemical modeling, anthropogenic carbon, oxygen, compound change

Key points:

1. Surface and bottom water rates of change differ for carbon NWA shelf variables.
2. The largest local anthropogenic carbon content is found in the southern MAB shelf.
3. The largest DIC accumulation is in the Gulf of Maine due to coastal modification.
4. Under SSP5-8.5, trends accelerate, and modification continues.
5. Under SSP5-8.5, trends differ in surface and bottom waters.

Abstract:

Increasing atmospheric carbon dioxide concentrations are accompanied by ocean acidification, oxygen loss, and warming of the global ocean. However, in coastal environments, local processes that occur on small spatial scales can moderate or exacerbate these trends. These processes are not well represented in global climate models. Therefore, downscaled tools are useful to decipher carbonate system drivers and predict conditions. Here we describe the application of a ROMS based regional model of the northwest Atlantic shelf, stretching from Florida to Newfoundland, with ~7 km horizontal resolution. The biogeochemical model relies on the Carbon, Ocean Biogeochemistry and Lower Trophics (COBALT) model in combination with regional empirical models to reconstruct the carbon variables. Using a 30-year historical simulation, model results are evaluated against in situ observations and then used to estimate anthropogenic carbon inventories for the region. Historical trends differ between surface and bottom conditions with bottom trends identified as more severe. Circulation and changes in the water column metabolism amplify local rates of change historically, while warming and water mass changes act to dampen these changes. Regional locations of accelerated carbon storage and accumulation are identified and described to be modified by coastal processes. A time-varying dynamic delta forced future projection out to 2098 under SSP5-8.5 projects how these trends will continue and indicates future acceleration of trends. Observing compound change, or multiple stressors changing in concert or closely, requires not only over-constraint on the carbon cycle parameters, but also multiple co-existing biogeochemical observations to refine the mechanisms responsible for local climate variability.

Introduction:

Over recent decades, the combination of fossil fuel emissions, deforestation, and cement production have imparted large physical and biogeochemical modifications on the world's oceans [Le Quéré et al. 2018; Gattuso et al. 2015]. The global average patterns of the oceans have gotten warmer and salinity distributions have been altered with density structures and stratification patterns modified [Talley et al. 2016]. Biogeochemical alterations are also occurring, including oxygen declines, changes in productivity, and increased dissolved inorganic carbon content due to uptake of anthropogenic carbon dioxide – which alters the pH and mineral saturation state (Ω) of calcium carbonate through a process called ocean acidification (OA) [Doney 2010; Bopp et al. 2013]. This compound change– that is, multiple stressors changing in concert or closely - is happening at different rates and magnitudes across the globe including coastal waters.

In coastal waters, local processes are further modifying the compound change and causing it to occur at different rates than observed globally [Gledhill et al. 2015; Siedlecki et al. 2021a, 2021b]. Most coastal areas have experienced significant increases in sea surface temperature (SST) at an overall rate of 0.25°C per decade from 1982 to 2010 [Lima and Wethey 2012], which exceeds the global average SST trend of ~0.095°C per decade from 1979–2012 [Hartmann et al. 2013]. In the Northwest Atlantic, high-resolution projections under doubling of CO_2 warmed nearly twice as fast as the coarse resolution global simulation for the same region [Saba et al. 2016]. Two high-resolution downscaled projections under RCP8.5 forced by 4 different global climate models were compared out to 2050 [Brickman et al. 2021]. They found that the SST rates of warming exceeded the observed 100-year rate of warming for all the ensemble members. Three of the four global models predicted freshening of surface waters, and stratification increased in all simulations [Brickman et al. 2021]. All these studies attributed the increased rate of warming on the shelf relative to the basin to shifts in circulation and/or atmospheric changes altering warming patterns [Saba et al. 2016; Alexander et al. 2020; Brickman et al. 2021].

Atmospheric carbon dioxide has increased at a rate of 2-3 ppm per year [Le Quéré et al. 2018], and surface waters in the open ocean have mostly followed this long-term trend, effectively keeping up with the rising atmospheric concentrations. Previously, the partial pressure of carbon dioxide (pCO_2) in coastal shelf waters has been shown to lag the rise in atmospheric CO_2, unlike the open ocean [Laruelle et al. 2018]. However, some regions amplified the global uptake, while others did not keep up with the atmosphere or dampened the global signal. For example, over the past 15 years, waters in the Gulf of Maine (GOM) have taken up CO_2 at a rate significantly slower than that observed in the open oceans due to a combination of the extreme warming experienced in the region and an increased presence of well-buffered Gulf Stream water [Salisbury and Jönsson 2018]. The reduced uptake of CO_2 by the shelves also alters local acidification rates, causing them to diverge from the global rates.

Several high resolution simulations were used to project OA conditions to 2050 [Siedlecki et al., 2021]. By 2050 under the RCP 8.5 projected climate scenario, saturation states of aragonite (Ω_a) declined everywhere in the GOM and the region experience conditions below the critical Ω_a threshold of 1.5 for most of the year by 2050 [Siedlecki et al., 2021]. Despite these declines, Siedlecki et al. (2021) determined the projected warming in the GOM imparts a partial compensatory effect to Ω_a by elevating saturation states considerably above what would result from acidification alone, pointing to the need for a more comprehensive view of changing ocean conditions.

In addition to regional warming altering OA rates, changes in water masses and circulation patterns [Gonçalves Neto et al., 2023; Jutras et al., 2023; Townsend et al., 2023; Balch et al., 2022; Gonçalves Neto et al., 2021; Claret et al., 2018; Mills et al., 2013; Pershing et al., 2015] also locally modify OA rates. Water mass influences were critical to the recent analysis of Li et al. (2024) who identified regional rates of anthropogenic carbon accumulation on the U.S. East Coast using observations. Their analysis revealed the slope waters have the highest accumulation rate in the region and identified the shelf as a critical region of export of anthropogenic carbon to the open ocean. This process of export would reduce the stress locally of additional carbon storage helping to alleviate some of the stress of OA.

The intrusion of anthropogenic CO_2 is not the only mechanism that can reduce Ω_a within coastal surface waters. Local processes like freshwater delivery, eutrophication, water column metabolism, and sediment interactions can also modify regional variability in Ω_a [Cai et al., 2011; Siedlecki et al., 2017; Qi et al., 2017; Pilcher et al., 2018; Feely et al., 2008; 2018; Siedlecki et al., 2021a,b]. Global projections cannot resolve these local processes with resolution of a degree or more. High-resolution global projections have been developed which perform well in some coastal settings with physical variables only [Saba et al., 2016] and with biogeochemistry [Ross et al., 2023]. However, these projections simplify regional biogeochemical processes described above which can amplify or dampen these global changes, particularly in coastal shelf regions.

Understanding and projecting changes on decadal-centennial timescales is critical for regional fisheries. The time scale of regulations, business decisions, and investments for regional fisheries tends to occur at decadal scales: e.g., vessel or infrastructure built up in response to an emerging or recovering fishery [Fryxell et al., 2010; Steele 1998; Tomassi et al., 2017]. Organismal thresholds in pH or Ω will likely be exceeded by 2050 in the GOM in subsurface environments, but more certainly by the end of the century based on projections using CMIP5 global models under the most aggressive emissions scenario [Rheuban et al., 2018; Siedlecki et al., 2021]. To address these issues, in this study, we forced an existing regional model with the most recent simulations performed in the framework of the Coupled Model Intercomparison Project 6 [CMIP6, Stockhause et al., 2021]. In doing so, we assessed how these modified ocean fields continue to evolve over the course of the 21st century. Regionally downscaled climate projections of multiple climate-associated stressors (temperature, oxygen, pH, Ω, and pCO_2) are produced to simulate both the past 30 years and provide continuous 100-year projections for the U.S. East Coast under the SSP5-8.5 emission scenario [Kriegler et al., 2017]. We present our findings of compound change with a focus on the important benthic regions hosting the US and Canadian scallop fisheries as this region has been previously identified as vulnerable [Hare et al., 2016]. In addition we generated inventories of anthropogenic carbon spatially and will explore how the spatial gradient in the uptake of carbon locally influences trends in carbon variables both historically and into the future.

Background oceanography and projections in the region:

The coastal ocean off the east coast of the US is home to valuable fisheries, a significant proportion harvesting calcifying organisms [Cooley and Doney, 2009]. The eastern U.S. continental shelf is comprised of three major subregions. To the north is the GOM, which extends from the Scotian shelf to Cape Cod. The GOM receives significant freshwater input from the local rivers and relatively fresh and cold water from the Labrador Current, a southward-flowing buoyancy-driven coastal current originating on the coast of Greenland [Townsend et al., 2004; 2015]. The Labrador Current's water enters through the Northeast Channel where it continues in a counterclockwise circulation path and has demonstrated significant variability on decadal time scales [Townsend et al., 2004; 2015].

To the south of Cape Cod is the Mid-Atlantic Bight (MAB), which extends to Cape Hatteras. Its shelf and slope waters maintain a salinity below 34 as a result of significant freshwater contributions [Townsend et al., 2004]. Exchange with the slope water is modulated by the existence of a persistent shelf break front, which can be punctuated by meanders and intrusions of warm, salty water from the northward-flowing Gulf Stream, as Figure 1 shows [Joyce et al., 1992; Chen et al., 2014; Zhang and Gawarkiewicz 2015, Townsend et al., 2004]. Beneath the thermocline in the summer, the cold winter water is trapped subsurface and is known as the "Cold Pool" [Houghton et al., 1982; Loder et al., 1998]. Results from historical simulations using the same NWA-ROMS model used in this study, suggest that the Cold Pool originates not only from local remnants of winter water near the Nantucket Shoals, but has an upstream source transported in the springtime from Georges Bank along the 80-m isobath [Chen et al., 2018]. Ocean temperature variability on the northeast US (NEUS) continental shelf has been linked to large-scale ocean circulation from the Gulf Stream [Nye et al., 2011], with advection from the Labrador Sea also having major impacts on the downstream temperatures [Chapman and Beardsley 1989; Rossby and Benway 2000; Shearman and Lentz 2010; Xu et al., 2015].

Observations in combination with results from a high-resolution global climate simulation identify a long-term decline in oxygen concentrations and attribute this to a retreat of the Labrador Current associated with the slowdown of the Atlantic Meridional Overturning Circulation (AMOC) [Claret et al., 2018]. Nguyen et al. (in revision) used observations below the regional mixed layer to determine the rate of oxygen decline over the shelf and identified Apparent Oxygen Utilization (AOU) as the dominant driver of the decline. The changes in AOU could be driven by local changes in water column metabolism or by circulation shifts in the region.

Methods:

Historical run description: The physical ocean circulation model used for this study is the Regional Ocean Modeling System (ROMS), with horizontal curvilinear and vertical terrain-following sigma coordinates [Shchepetkin and McWilliams 2005]. The model domain covers the entire Northwest Atlantic (NWA), including the NEUS shelf, slope, and the major path of the Gulf Stream [Kang and Curchitser, 2013; Zhang et al., 2018; Chen et al., 2018]. The grid is configured with horizontal spacing of ~7 km and 40 vertical terrain-following levels stretched toward the surface, with the highest resolution of 0.24 m near surface and the lowest resolution of 250 m at depth offshore. The biogeochemical module called the Carbon, Ocean Biogeochemistry and Lower Trophics (COBALT) model [Stock et al., 2014] developed by NOAA GFDL has been incorporated into ROMS and used to evaluate the lower trophic level and nitrogen budgets for the NWA region [Zhang et al., 2018; Zhang et al., 2019]. The model has been shown to skillfully simulate variability in water masses entering GOM in terms of T and S and to skillfully represent variability in chlorophyll [Chen et al., 2018; Zhang et al., 2019]. The historical simulation was forced by atmospheric reanalysis, so comparisons with observations direction can be performed and the skill evaluated directly.

Because the COBALT generated DIC, Alk was not skillful (not shown), we then applied empirical models, specifically a Multiple Linear Regression (MLR) of the carbonate system parameter based on hydrographic variables (T, S, and O_2, equation V- see McGarry et al., 2021), and added observed anthropogenic carbon trends from the North Atlantic as described in Siedlecki et al. (2021b). The results described in Siedlecki et al.

(2021b) showcased how well this approach represented the seasonal cycle of surface aragonite saturation state in the GOM and the results here are evaluated more below. In addition, the results compared well with the Canadian team projections using a coupled dynamic carbon model. We found the total alkalinity (TA) estimates from McGarry et al. (2021) performed better within the region, so we only used those. Finally, as an alternative to McGarry, we also experimented with Empirical Seawater Property Estimation Routines-Neural Networks (ESPER-NN) equation 7 [Carter et al., 2021], which includes estimates of anthropogenic carbon over time. Dissolved inorganic carbon (DIC) was calculated with equation VII which uses T, S, and O_2 to estimate dissolved inorganic carbon. The code requires in situ temperatures as inputs then ROMS potential temperature fields were converted with the Gibbs-SeaWater Oceanographic toolbox for MATLAB, version 3.06.12 [McDougall and Barker, 2011]. By passing the time variable to the calculations, ESPER estimates the anthropogenic carbon added to the ocean and compared with recent observation-based estimates for the region (Li et al. 2024). Similar to the prior MLR application described in Siedlecki et al. (2021b), the carbon equilibrates with the MLD using the simulated surface temperatures and salinities in addition to the empirical model additions. Anthropogenic carbon inventories are estimated by accumulating the volume-weighted sum of the ESPER-derived value over the shelf through the end of 2014, where the historical simulation ends.

Apparent Oxygen Utilization (AOU) is calculated as the difference between oxygen solubility and the in situ oxygen concentration:

$$AOU = O_{2,solubility} - O_{2,in\ situ} \quad (1)$$

AOU reflects the cumulative effect of water column metabolism and the pre-formed O_2 concentration of the source waters, as AOU changes with changing circulation and residence times as well [Ito et al., 2017]. Positive AOU is interpreted as oxygen is consumed or depleted due to increased consumption of organic material, decreased mixing, and/or circulation changes with more influence from water masses with higher AOU. Organic matter consumption also generates DIC and reduces TA.

Future forcing generation: *Time varying projections driven by CMIP6 model output*

While CMIP6 shares many features with previous intercomparison projects, it is redesigned using a new more structured system (see Eyring et al., 2016). Here we use a climate model driven by the SSP5-8.5, which is similar but not identical to the RCP8.5 scenario in CMIP5. While the SSP5-8.5 scenario is considered a “no policy” scenario and exceeds currently emission reductions planned with current global policies, it is unlikely to occur (Hausfather & Peters, 2020) but not impossible (Christensen et al. 2018; Sarofim et al. 2024). Here we chose to employ this notably high-end scenario to explore if ocean acidification thresholds could be surpassed for the region if at all, as this was a question raised by the community when we started this work. As scenario uncertainty collapses prior to 2050 and natural variability dominates before then (Hawkins and Sutton, 2009; Deser et al. 2012; 2014), this extreme scenario choice is most influential for the projection period beyond 2050.

We examined the set of the global earth system model simulations in CMIP6 using SSP5-8.5 and chose the GFDL ESM4 model, which has a relatively high atmospheric resolution (~1° lat x 1° lon) and well-developed ocean physical and biogeochemical components. The GFDL ESM4 also uses COBALT, enabling a more seamless passing of ocean conditions at the ROMS boundary.

To retain both the mean climate and high-frequency variability from observations, a method was employed that removes the mean bias and retains realistic unforced climate variability over a range of time scales. Following Pozo-Buil et al. (2021) we use a “time-varying delta” method based on output from the GFDL ESM4 simulation combined with values obtained from renalyses. The "deltas" are time varying using 3 hourly data from the atmosphere using the following equation:

ATM' (1980-2100) = REAN_CLIM + DELTA (2)

where REAN_CLIM was generated from the Japanese 55-year Reanalysis based surface dataset for driving ocean-sea ice models (JRA55-do) forcing files from 1980-2014 [Tsujino et al, 2018], which was used to generate the historical simulation [Zhang et al., 2019]. Because JRA55-do is a surface dataset for driving ocean-sea ice models, it has NAN values over land regions and values only over the ocean. The atmospheric REAN_CLIM was interpolated to the DELTA grid and "not a number" or NANs in the air temperature (Tair) and humidity (Qair) DELTAs were replaced using extrapolation.

The daily mean historical annual cycle (4 harmonics) + daily averaged delta for rain, shortwave, and longwave radiation deltas were smoothed to a daily resolution atmospheric forcing. The atmospheric forcing files (for all variables) was computed as the smoothed time series plus the delta. Atmospheric CO_2 forcing was calculated using the monthly average from the forcing file used in the historical simulation, and then adding the respective Delta from SSP5-8.5 for each year.

The dynamic time-varying delta ocean forcing was generated using monthly data for the ocean climatology forcing and boundary conditions using the following equation:

OCN' (1980-2100) = REAN_CLIM + DELTA (3)

Where the REAN_CLIMs for the ocean were generated using the SODA3 ocean reanalysis as described in Zhang et al. (2019). The ocean REAN_CLIMs were interpolated to the ROMS 3D coordinates. All DELTAs were interpolated to the ROMS grid and NANs in the DELTA files were replaced via interpolation using nearest. The forcing is computed in this manner, rather than using the original fields from the earth system models, to remove the mean bias in the latter (e.g., the NE US coast tends to be too warm in most climate & earth system models).

The physical and biogeochemical values have been applied to ROMS-COBALT in the forcing at the surface and side boundaries directly from GFDL's ESM4 output for Nitrate, Silica, and Oxygen. Phosphate and other variables utilized the same forcing as in the historical which was the WOA climatological condition [Zhang et al., 2018]. Because the historical simulation used the climatological conditions that were disconnected from the other water properties, we could not use the same delta approach as we had done with other variables. The carbon variables were reconstructed after the run was completed using statistical empirical relationships as described in the historical section above.

The surface fields include winds, air temperature, humidity, and CO_2, while the ocean fields include temperature, salinity, currents, alkalinity, DIC, nitrate, oxygen, and silicate, where the biogeochemical fields are required to be greater than zero and the biological fields adjust rapidly to the imposed forcing. Freshwater flux into the ocean from major rivers is applied at the locations identified in the Dai et al. (2009) database using the historical forcing described in Zhang et al. (2019). We assume the flux of freshwater remains constant in the future simulations.

Observations used for oxygen and carbon variable evaluation:
Oxygen observations from the World Ocean Database (WOD18; Boyer et al. 2018) were collated for evaluation with model fields from 1980 to 2014. WOD18 observations include bottle samples (Ocean station data, OSD), as well as CTD sensors. In addition, a mooring (A1) from the Gulf of Maine in 51 meters of water depth spanning 2002 to 2014, was also utilized for model evaluation.

Although the US East Coast and Gulf of Mexico are some of the best studied ocean regions in the world [Townsend et al., 2004], measurements of carbonate system parameters are sporadic, but were recently compiled in a data curation, CODAP-NA [Jiang et al., 2021]. The Gulf of Mexico and East Coast Carbon (GOMCC) cruises measured DIC, TA, and pH in July-August 2007, 2012, and 2017 [Wang 2013, Wanninkhof, 2015]. The East Coast Ocean Acidification Cruise (ECOA) measured these parameters in June-July 2015 [Xu et al., 2017], again in 2018, and in 2022. Carbonate parameters, analyzed at AOML, are also taken on surveys (ECOMON) conducted by NOAA NEFSC over the continental shelf from Cape Hatteras, NC to Cape Sable, NS. Canadian data from the Atlantic Zone Monitoring Program (AZMP) includes carbonate parameters from the Gulf of St Lawrence, Quebec, Maritimes, Newfoundland and Labrador which are critical for understanding the slope water formation influencing our region. Additionally, ten brief cruises each lasting 1-2 days were conducted on the RV Tioga between 2013-2015, covering only the Wilkinson Basin region in the southwestern GOM [Wang et al., 2017]. DOE OMP cruise EN279 data from March 1996 [Huang et al., 2021] was also used for reference.

Model skill evaluation

Because the simulation has been used previously, we rely on those prior efforts to evaluate the lower trophic level and nitrogen budgets for the NWA region [Zhang et al., 2018; Chen et al., 2018; Zhang et al., 2019]. We focus on evaluation of oxygen from COBALT and carbon variables from the empirical relationships in this paper. Three metrics are used to evaluate model skill: the Pearson correlation coefficient (R-values), normalized root mean squared error (NRMSE), and the normalized bias (NB) with a range characterizing the performance as "Excellent," "Reasonable," and "Poor" following the definitions found in Allen et al. (2007) and Kessouri et al. (2021). As the r-values approach 1, the phasing between the two temporal signals is in agreement; note however that this metric alone does not indicate the correspondence between the magnitudes of the two signals. The SD is influenced by both the phasing of the series and how well the hindcast variability compares with the observed variability. The NRMSE here represents the RMSE normalized by the standard deviation of the observations. If the model and observations are close to each other, the RMSE will be small, and consequently the standard deviation will be close to 1 and values then are categorized as: <0.2 excellent; 0.2–0.4 reasonable; and > 0.40 poor. The NB (model bias normalized by the data) quantifies the apparent bias in the model and values are categorized as: <0.2 excellent; 0.2–0.4 reasonable; and > 0.40 poor [Maréchal, 2004].

Statistic	*Excellent*	*Reasonable*	*Poor*
Pearson correlation coefficient	1-0.8	0.8-0.5	<0.5
NRMSE	<=|0.2	|0.2-0.4|	>|0.4|
Normalized Bias (Marechal, 2004)	<=|0.2|	|0.2-0.4|	>|0.4|

Table 1: Statistical ranges defining our descriptions of model performance modeled following the approach described in Kessouri et al. (2021).

Trend analysis:

The linear trends presented here were obtained by calculating the linear least-squares regression at each single grid cell from yearly averaged time series: historical as 1980-2014 and future as 2015-2098. This results in the generation of two-dimensional arrays of trends (rates of change) for bottom and surface, as well as depth-integrated volume-weighted fields.

Attribution analysis:

To identify the drivers of historical change to the change in DIC content in the historical simulation, we utilized the empirical carbon model capabilities. The depth-integrated DIC trend was separated into the anthropogenic carbon contribution, the thermal contribution, and the salinity contribution. The anthropogenic carbon contribution isolated the year term in the ESPER-NN equation and allowed the atmospheric CO_2 concentrations to be in equilibrium with surface waters down to the mixed layer depth. The thermal contribution was isolated by comparing the base simulation with a simulation performed using only the temperature from the first decade repeated over 3 decades. The first decade of temperatures is cycled through the entire time series and then differenced with the historically reconstructed DIC trend. Similarly, the salinity contribution was isolated by comparing the base simulation with a simulation performed using only the salinity from the first decade repeated over 3 decades. The first decade of salinity is cycled through the entire time series and then differenced with the historically reconstructed DIC trend.

Results:

Model Evaluation

Oxygen: Overall, the spatial variation in time of bottom oxygen conditions on the NWA shelf are *reasonably* well simulated. Oxygen changes spatially compare *reasonably* well with *r*-values falling into the *reasonable* category (r=0.57; Figure S1-S3), the phasing of the temporal variation in is *reasonably* well simulated as diagnosed by NRMSE (0.24), oxygen was biased low on average but *excellent* (NB = 0.20) over most of the domain pictured in Figure 1. When compared against the trend from WOD in the 50-100 m depth bin reported in Nguyen et al. (*in review*), the modeled oxygen is biased high (Figure S4). The source of this bias appears to be mostly the AOU contribution as that is biased low over most of the domain (Figure S5, NB =0.49). Although the established temperature bias [du Pontavice et al., 2023, Chang et al., 2021, Chen and Curchitser, 2020] contributes to the overall bias as well, solubility is much better simulated than AOU trends (Figure S5-S6). Despite these biases, the trend is *reasonably* well (r= 0.57) simulated over the course of the simulation in the subsurface outer shelf region (50-100 m; Figure S4). Given our approach, we expect these biases to impact DIC and TA and discuss the specifics of that in the section evaluating those variables below.

Variable	*Correlation Coefficient (CC, r)*	*NRMSE*	*Normalized Bias (NB)*
Oxygen WOD	*0.57*	*0.24*	**0.20**
AOU WOD	*0.55*	0.53	0.49
DIC_{MLR}	**0.91**	**0.01**	**0.01**
TA_{MLR}	**0.89**	**0.02**	**0.01**
$\Omega_{arag-MLR}$	**0.83**	**0.2**	**0.16**
$\Omega_{calcite-MLR}$	**0.83**	**0.19**	**0.15**
pCO_{2-MLR}	*0.56*	**0.15**	**0.12**
pCO_{2-MLR} Mooring	*0.56*	**0.18**	**0.16**
DIC_{ESPER}	**0.91**	**0.01**	**0.01**
TA_{ESPER}	**0.89**	**0.02**	**0.01**
$\Omega_{arag-ESPER}$	**0.83**	0.2	0.16
$\Omega_{calcite-ESPER}$	**0.83**	0.19	0.15
$pCO_{2-ESPER}$	*0.58*	0.15	0.12
$pCO_{2-ESPER}$ Mooring	0.11	0.25	0.2

Table 2: Summary of the three model evaluation statistical metrics of performance used in this work for all the carbon and oxygen variables explored in the results. Results for both the MLR from McGarry et al (2021) and ESPER-NN [Carter et al. 2021] based approaches to reconstructing carbon variables are showcased. Excellent values are bold, while reasonable are italicized and poor are unformatted.

Carbon variables

Overall, the spatial variation in time of dissolved inorganic carbon (DIC) conditions on the NWA shelf are *excellent* over the period of the observations (2007-2014). DIC changes spatially compare well with r-values falling into the *excellent* category for both the MLR and the ESPER based approaches (r=0.91; Table 2), and the phasing of the spatial variation in time well simulated as diagnosed by NRMSE (0.01 for both, Table 2). In general, DIC is biased slightly high in the simulation (Figures S4 and S5; 6 μmol/kg), but still its performance falls into the *excellent* range for NB (0.01, Table 2). When compared with observations from 1996 (Figure S16), the simulated model skill remains *excellent*. Despite the AOU bias in the simulation, DIC appears to be well simulated.

Similar to DIC, TA's performance over space and time also falls into the *excellent* category in general. TA spatial and temporal variation compare well with R-values falling into the *excellent* category (r=0.83-0.89) for both the MLR and ESPER based approaches, and the phasing of the spatial variable was well simulated as diagnosed by NRMSE (0.01, Table 2). TA is biased slightly high in the simulation (Figures S6, S7; Table 2), but its performance still falls into the *excellent* range for NB (0.01, Table 2).

Saturation state (Ω) for calcite and aragonite both perform similarly, also falling into the *excellent* category. Ω changes spatially compare well with r-values falling into the *excellent* category (r=0.83, Table 2) and performing similarly between the MLR and ESPER approaches. The phasing of the signal spatially and in time was also well simulated (*excellent*) as diagnosed by NRMSE (0.2, Table 2). Ω is biased low in the simulation (NB =0.15-0.16, Table 2; Figure S8-11) The increase in bias is likely due to the bias in temperature already established in the simulation.

pCO_2 performs *reasonably* in the simulation with the weakest statistics overall. The spatial and temporal variation compares reasonably well with r-values falling into the reasonable category (r=0.58, Table 2, Figure S12, S13) for both ESPER and MLR based approaches. The phasing of the signal as well simulated in space and time as diagnosed by NRMSE. pCO_2 is biased slightly high with a NB of 0.12-0.2 (Table 2) falling into the *excellent* category. Despite this weakness, the simulation seems to perform reasonably for this variable, giving us confidence to move forward with the projections and further analysis of the results.

Annual climatology

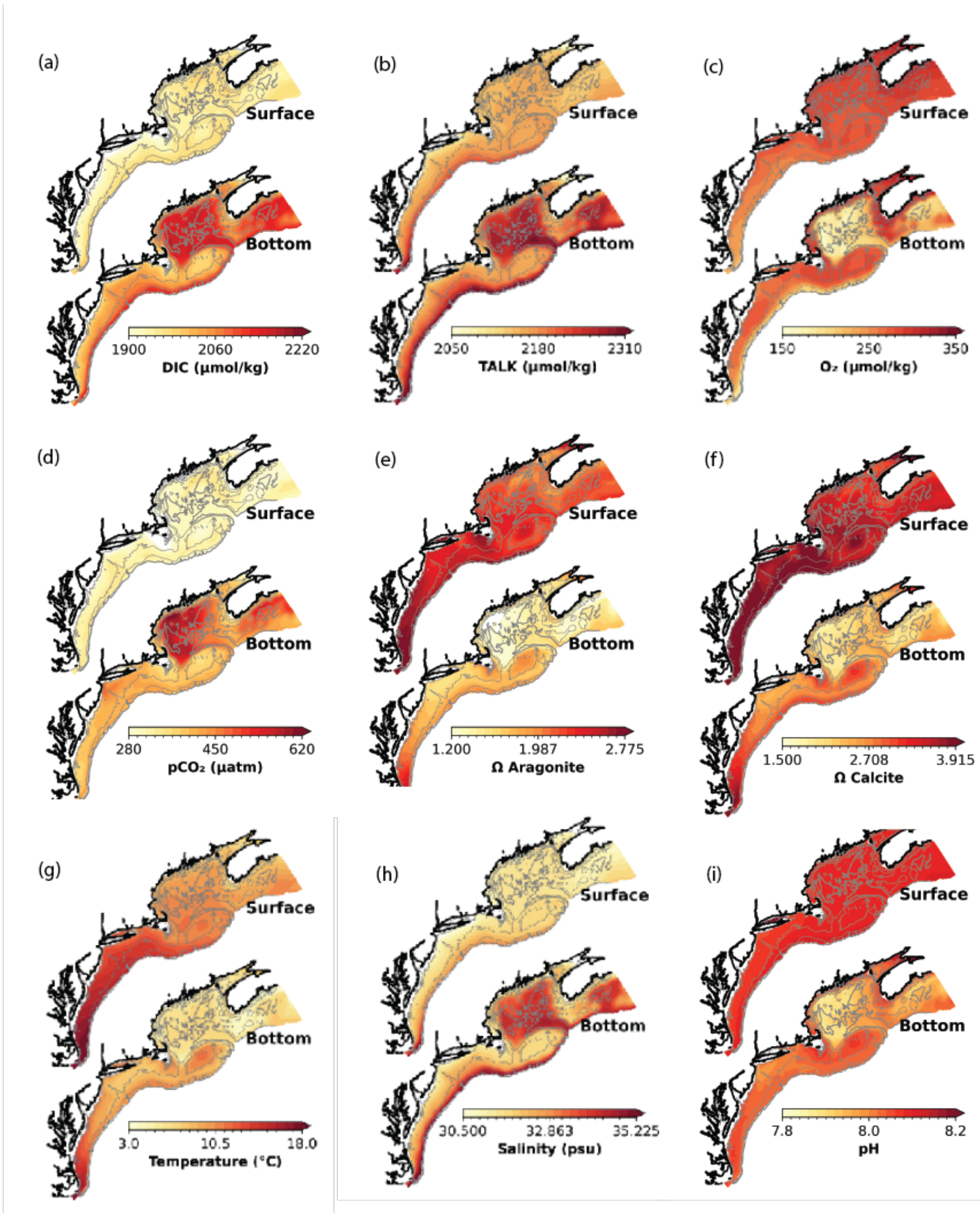

Figure 1: Climatological maps (1981 to 2014) of simulated surface and bottom conditions on the NWA shelf within the model domain. (a) DIC (μmol/kg), (b) TA (μmol/kg), (c) oxygen

(μmol/kg) (d) pCO_2 (μatm), (e) Ω_{arag}, (f) $\Omega_{calcite}$., (g) temperature (deg C), (h) salinity (psu), and (i) pH on the total scale.

Bottom DIC concentrations vary from 1900 to 2300 μmol/kg over the region on average (Figure 1a). The deeper locations house more carbon with the GOM and Gulf of Saint Lawrence containing the highest concentrations of DIC. The difference between the most recent decade simulated (2001-2010) and the earliest decade simulated (1981-1990) identifies regions where the DIC has changed the most. These include the deep Wilkinson Basin in the GOM, the outer shelf, and the region south of the Hudson River outflow off the coast of New Jersey.

TA ranges from 2050 to nearly 2300 μmol/kg and is lower at the surface than at the bottom (Figure 1b). Offshore waters tend to be highest in TA, consequently the deep Wilkinson Basin and the outer shelf experience the highest TA at the bottom. The lowest TA occurs at the surface and in the northern edges of the domain. Notably, TA increases further south in the domain on the shelf.

Bottom oxygen concentrations vary from 100 to 350 μmol/kg on average (Figure 1c). The lowest concentrations are found in the deepest locations (e.g., Wilkinson basin, Scotian Shelf, and on the outer shelf of the MAB). The highest values are found in the further north regions of the domain in the shallow shelves within the Gulf of St. Lawrence and off the coast of Newfoundland. Bottom oxygen decreases the most over the multidecadal simulation in the Wilkinson Basin within the GOM, within the most interior portion of the Gulf of St. Lawrence, and off the coast of New Jersey.

AOU averaged annually over the 34-year historical simulation and then integrated over depth clearly highlights the recirculation occurring inside the GOM. AOU values exceed 65 μmol/kg in that region (Figure 2). The lowest AOU values occur in the southern portion of the MAB, and on Georges Bank. The Cold Pool region of the New York Bight is relatively higher than the surrounding shelf.

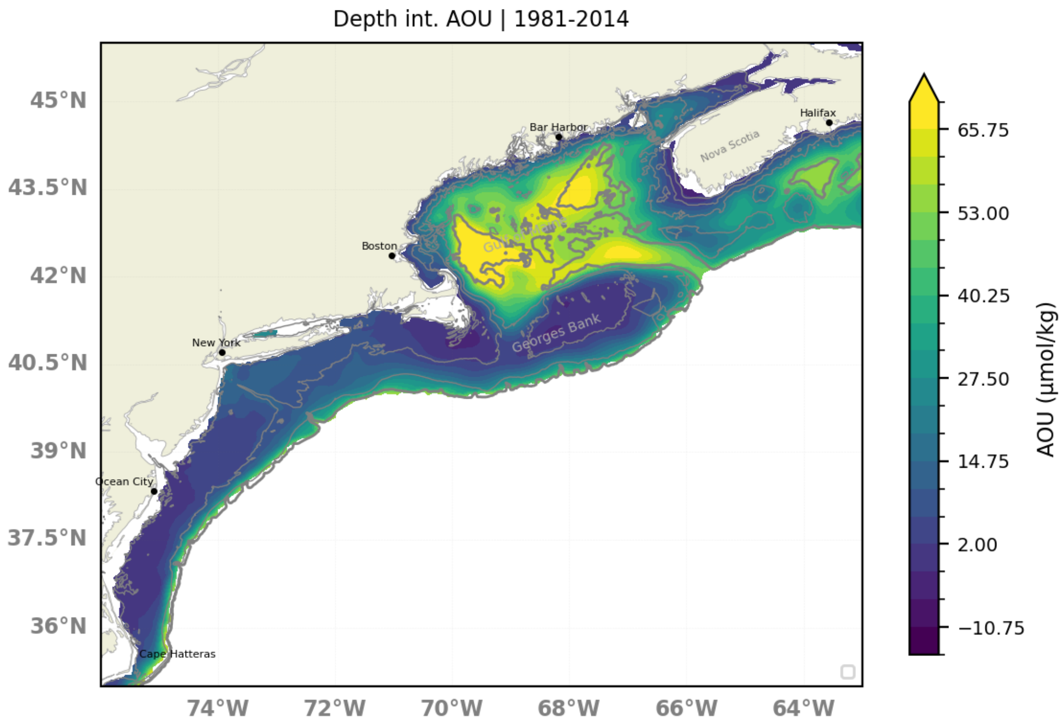

Figure 2: Climatological map (1981 to 2014) of depth integrated AOU for the NWA shelf region.

Bottom pCO_2 values range from 350 to 650 μatm on average with the highest values in the Wilkinson Basin in the GOM and inside the Gulf of St. Lawrence estuaries (Figure 1d). The lowest values can be found on the Georges Bank and some of the shallower shelves.

Bottom Ω is lowest in the deepest regions of the GOM, Scotian Shelf, and within the Gulf of St. Lawrence, with bottom values nearing saturation or becoming undersaturated (Figure 1e, 1f). The latitudinal gradient is also strong with the highest values in the southernmost region of the domain. Notably the outer shelf of the MAB as well as the rim of Georges Bank house the highest Ω. The saturation state was highest in the 1980s and lowest in the most recent time indicating a decline over the 34 years simulated with the MAB experiencing the greatest overall change. These results are the same for aragonite and calcite, but the magnitude differs in the change with the mineral saturation state.

The warmest waters are found at the surface in the MAB and the bottom waters in the southern regions of the MAB. The saltiest waters are found on the outer shelf and in the deep Wilkinson Basin in the GOM.

Bottom pH ranges from 7.8 to 8.1 in the region with the lowest values found in the Wilkinson Basin in the GOM and in the inner estuaries of the Gulf of St. Lawrence (Figure 1i). Some regions of the Scotian shelf also experience lower values. Bottom pH is highest in the 1980s and lowest in the early 2000s indicating a decline over this interval – in contrast to what is happening at the surface. The largest decline in pH occurs in the southern MAB region off the coast of New Jersey and Virginia.

Time rate of change- historical

Simulated salinity declined in both the surface and the subsurface over the period of the historical simulation (1981-2014, Figure 3g). A portion of this period has been observed to experience low salinities in the Gulf of Maine (2005-2010; Balch et al., 2022). On the Scotian shelf, the freshening trend was observed there historically (from 1975, Lehmann et al. 2023). Subsurface trends from observations switch to becoming saltier in 2010, while surface waters continue to freshen in the region [Lehmann et al. 2023]. The largest rates of simulated decline occurred in the southern portion of the MAB, where observations and trends of salinity have largely been unevaluated in the literature.

Temperature largely increases over much of the domain, except for the southern MAB region and deep Wilkinson Basin, which experiences some minor cooling. These patterns are sensitive to when the trends are calculated and, in this region, and notably most of the observed warming occurred near the end and after our simulation period (post 2008). This simulation has an established temperature bias [du Pontavice et al., 2023, Chang et al., 2021, Chen and Curchitser, 2020] which likely impacts the rest of this work as well.

Bottom oxygen concentrations decline over much of the region over the historical simulation period (Figure 3c). The region with the largest decline includes the regions closer to the coast inside the Gulf of St. Lawrence, Wilkinson Basin in the GOM, the northern portion of the Scotian shelf, and the New York Bight region.

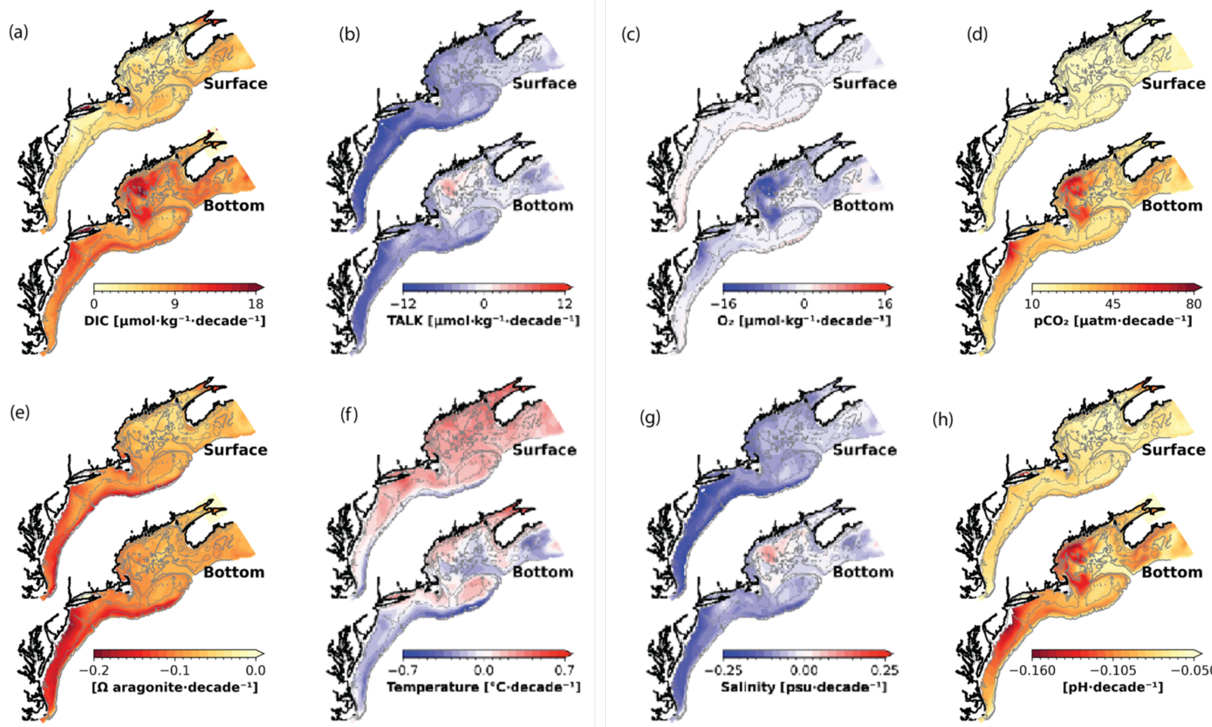

Figure 3: Maps of trends over 1981 to 2014 of surface and bottom conditions on the NWA shelf within the model domain. (a) DIC, (µmol/kg), (b) TA (µmol/kg), (c) oxygen (µmol/kg) (d) pCO_2 (µatm), (e) Ω_{arag}, (f) temperature (deg C), (g), salinity (psu), (h) pH on the total scale.

DIC is increasing more at depth (bottom) than at the surface with the largest rate of increase (18 µmol/kg/decade) occurring in the Wilkinson Basin, off the coast of New Jersey in the New York Bight, and along the outer shelf of the MAB. Meanwhile, TA is largely decreasing over much of the region with the largest declines occurring in the southern MAB. In Wilkinson Basin, however, TA is increasing at the bottom. Notably, the increases in DIC alongside declines in TA both have adverse effects on Ω, pH, and pCO_2.

pCO_2 increases over the entire region with the largest increases occurring at the bottom. The largest increases occur in the Wilkinson Basin and off the coast of New Jersey around the Hudson River in the New York Bight region (Figure 3d).

Ω declines over the entire region over this period with the largest declines happening at the bottom and in the southern portion of the domain at the surface (-0.2 units per decade). Bottom rates of decline are faster than the rates of decline at the surface, however the spatial patterns are similar. The GOM experiences the slowest decline in the area, but the climatological average of Ω is lowest in the north as well (Figure 1e-f).

At the A1 mooring in the GOM off the coast of New Hampshire, Ω is declining at a rate of -0.02 per decade (observed Trend, Figure 4) but the rate is not significant likely due to the high variability in the region. This rate, however, is similar to the rate observed for the N. Atlantic basin (-0.03 to -0.05 per decade; Jiang et al., 2015). This rate is also similar in magnitude but trending in a different direction than observations made at the surface from Buoy D in the GOM for 10 years (0.0152 ± 0.003 from 2004 to 2015, Salisbury and Jonsson 2018). However, the simulated trend is significant, and larger than the observed by a factor of 3 or so and is larger than that of the basin (Figure 4). Near the end of the observation from A1, there are data gaps (2011 to 2013) that coincide with lower Ω simulated in the simulation. These gaps are likely contributing to the differences between the simulated and observed trends. When the observed data set is stopped at 2011, before the gaps in the record but still 10 years of observations, the simulated and observed trends agree. As a result, with confidence in the simulated trends, we conclude that the subsurface decadal trends (0.1 per decade) exceed the basin-wide trends in the region (-0.03 to -0.05 per decade; Jiang et al., 2015). The record hovers around 1.5, which is a known threshold for organisms in the region

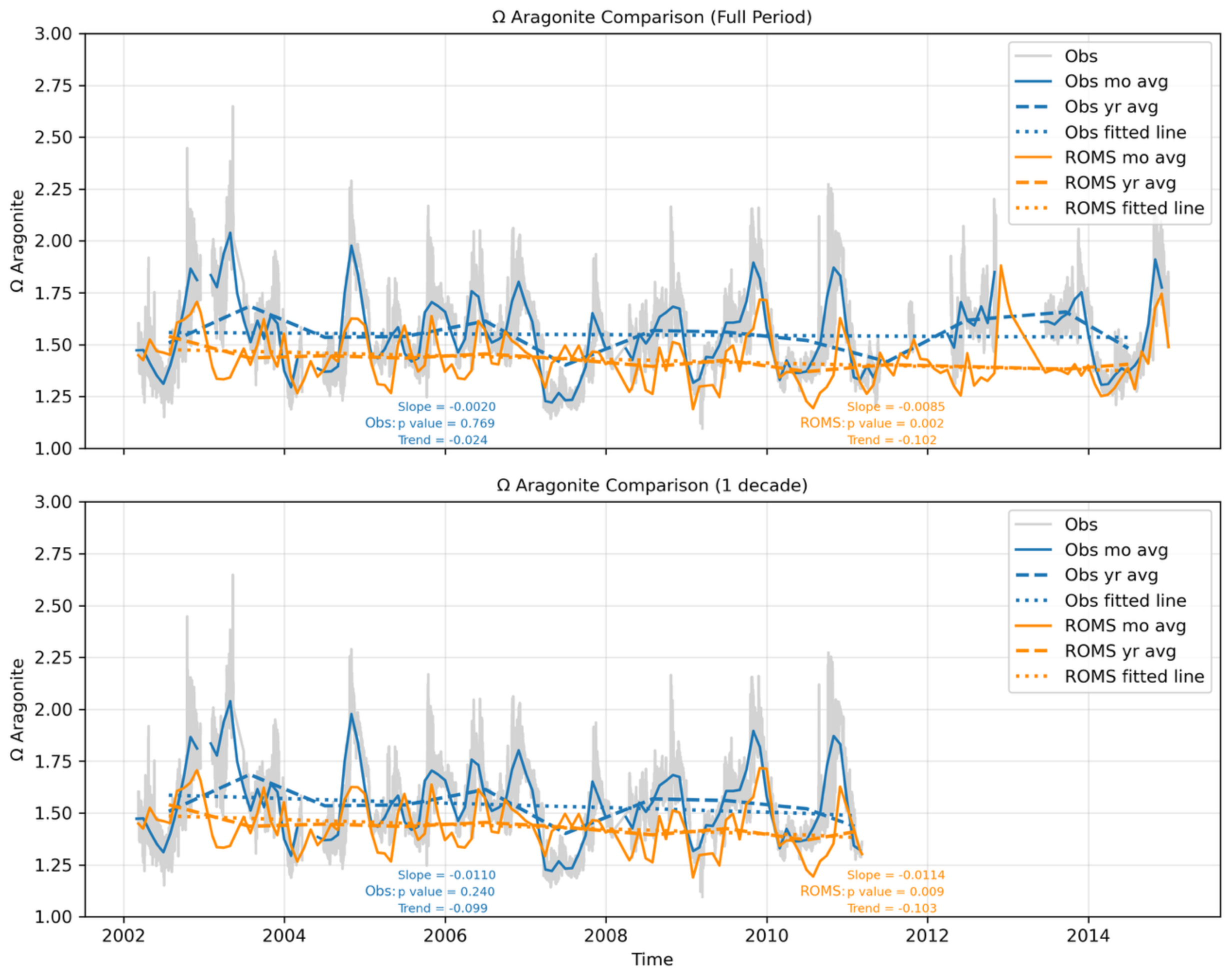

Figure 4: Reconstructed near-bottom trends of Ω_{arag} observed and modeled at mooring A1 in the GOM located 15 m above the bottom for the entire record (top) and solely the first decade of the record prior to the data gaps that begin in 2011 (bottom). The Ω_{arag} was reconstructed using ESPER-NN and the observed temperature, salinity, and oxygen time series from this subsurface mooring location. The observed time series was time-averaged monthly and annually as was the simulated ROMS output. The annual time series was fitted with a trend line and the resulting slope and trend are reported. Statistics identify a declining trend is observed (not significant) and simulated (significantly, $p<0.05$) in the region. The p-value is used to identify significance, the slope indicates the /yr difference using annually averaged input, while the trend quantifies the change over the entire time series (12 years). Notably, the simulated trend is larger than the observed by about a factor of 3.

Bottom pH is declining over the multi-decadal simulation over most of the domain except for the deep Gulf of St. Lawrence where a small area increases. The largest decline occurs in the southern MAB where pH declines by as much as 0.08 over 3 decades (Figure 3h).

Experiments with the observing strategy in the region (not shown) identify that the simulated observed change is best captured by increasing the frequency of monitoring in the region to annual summer cruises with the same sampling plan otherwise it's biased, especially in the GOM.

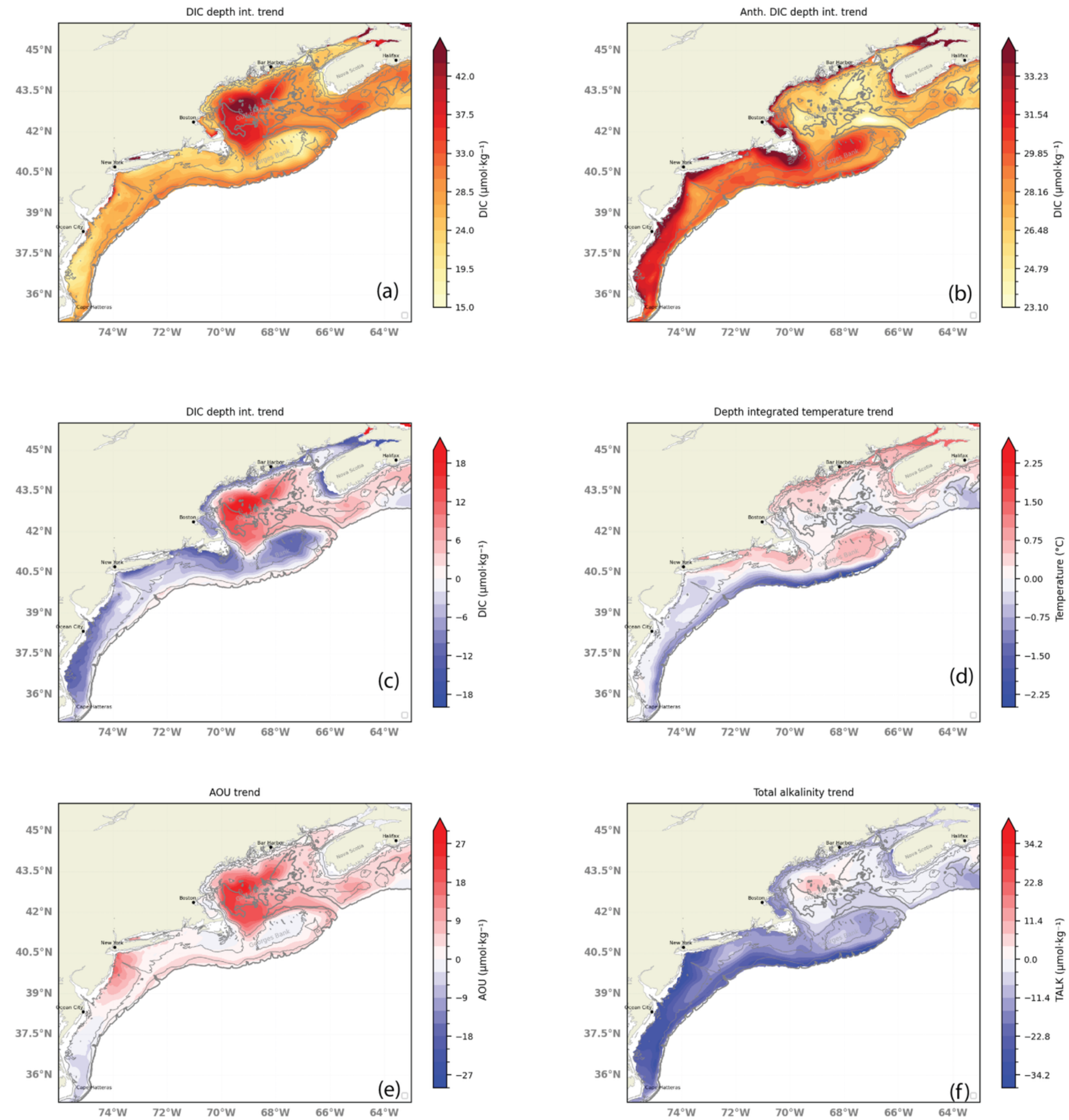

Figure 5: Maps of total change from 1981 to 2014 of depth integrated conditions on the NWA shelf within the model domain. (a) DIC (µmol/kg), (b) the anthropogenic "slug" of the DIC trend (µmol/kg) estimated with ESPER, (c) DIC without the anthropogenic "slug" of the DIC or (a)-(b) (µmol/kg), (d) Depth integrated temperature trends (deg C), (e) AOU trend (µmol O_2/kg), and (f) TA trend (µmol/kg).

Anthropogenic carbon inventory and historical compound change

The anthropogenic carbon inventory in 2014 relative to 1993 (Fig. 5B) varies spatially over the model domain with the highest inventory (34 μmol/kg) found in the regions closer to the coast in the MAB. The deeper and northern regions of the domain have lower inventories (~20-25 μmol/kg). The total DIC change over the realistically forced historical simulation (42 μmol/kg) is larger than anthropogenic carbon change (24 μmol/kg) in Wilkinson Basin, in particular (Figure 5 a-c). The change in the biological pump or the circulation changes in the region altering dominant water masses as identified by AOU, is amplifying the trajectory of the carbon variables in this region in some regions more than others (Figure 5e). The AOU change accounts for part of that difference (~20 μmol/kg C expected, Figure 5e) in the GOM. Other regions, like the MAB, the total DIC change is less than the anthropogenic carbon inventory suggesting other processes are reducing the DIC content in the region.

A better understanding of these patterns is obtained by breaking down the water column integrated DIC trends (Figure 6a) into the trend without the anthropogenic carbon (Figure 6b), the DIC trend difference due to the warming (Figure 6c) and the DIC trend due to the salinification patterns (Figure 6d). The model suggests that DIC would have declined in the MAB without the anthropogenic carbon dioxide. This decline is driven by the changes in temperature and salinity with salinity having a greater impact, but both stressors driving the DIC changes in the same direction. Both temperature and salinity changes over the last several decades have reduced the DIC content of the MAB region. TA also declines in response to this salinity trend in the MAB and contributes to a weaker uptake of carbon over most of the region (Figure 5f). The southern MAB and nearshore regions would have seen a larger DIC increase if the salinity trends over the first decade had remained constant historically. Similar patterns are found in the deep GOM. Temperature and salinity changes in the GOM have largely reduced the increase of DIC found in the region, but they are not the only contributors to the DIC trends. Notably the interior of the GOM experiences the largest increase in DIC and this is largely due to the AOU change in the region (Figure 5).

The northernmost region experiences the largest and fastest warming, while the southern MAB experiences the largest decline in TA at both the surface and the bottom.

Over the entire water column, AOU increases over many regions of the domain including the majority of the GOM and the region off the coast of New Jersey. The extreme values of AOU both get more extreme over the historical simulation suggesting AOU is accumulating in the deep GOM (Figure 5). In the southernmost region of the MAB, AOU declines, as it does over much of Georges Bank and along the coast. In addition, the region off the coast of New Jersey in the New York Bight area experiences the largest decline in oxygen and increase in AOU. All these factors contribute to the spatial pattern observed in the accumulation of anthropogenic DIC.

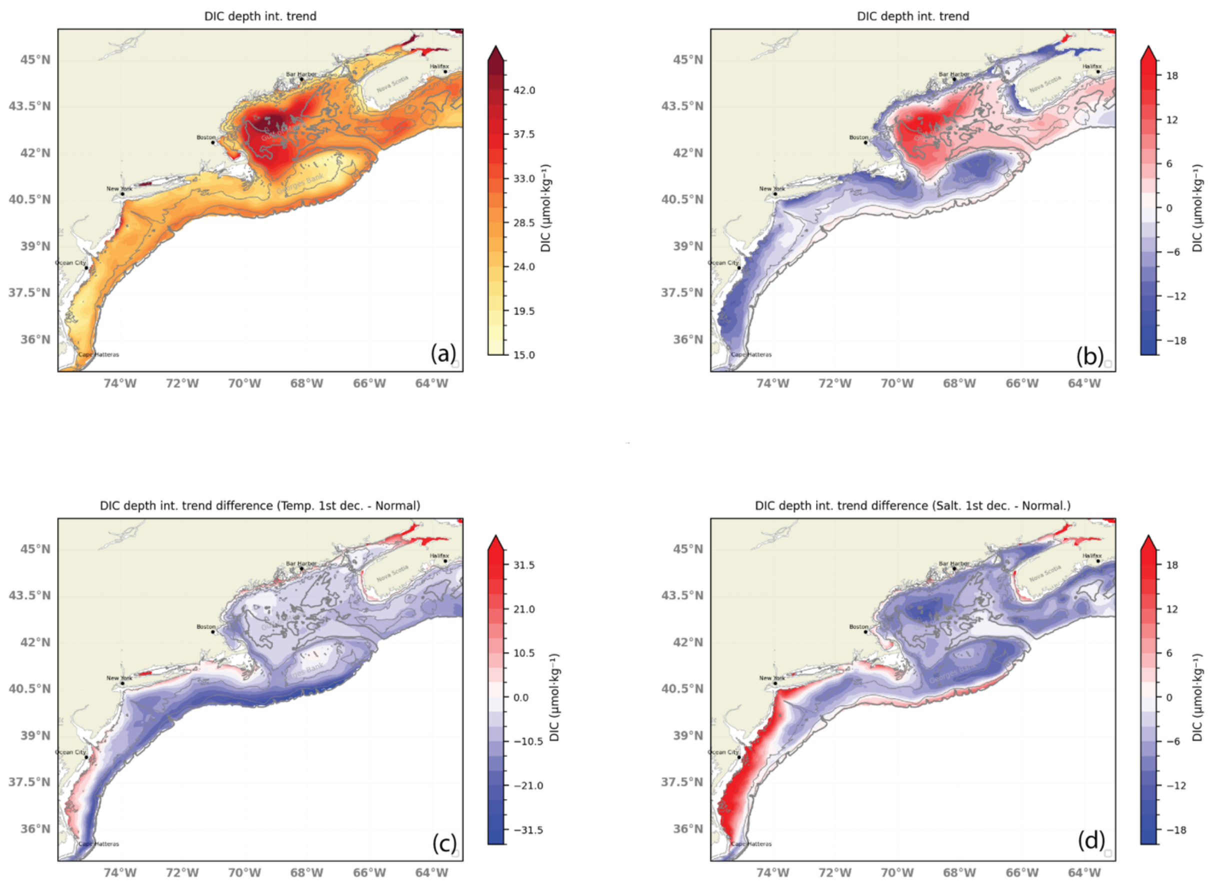

Figure 6: Maps of trends over 1981 to 2014 of depth integrated conditions on the NWA shelf within the model domain. (a) DIC (μmol/kg), (b) DIC without the anthropogenic "slug" or trend (μmol/kg), (c) DIC without the decadal change in temperature, i.e. the first decade of temperatures cycled through the entire time series and then differenced with the historically reconstructed DIC trend (μmol/kg), and (d) DIC without the decadal change in salinity, i.e. the first decade of salinity cycled through the entire time series and then differenced with the

historically reconstructed DIC trend (μmol/kg). In (c) and (d), regions that are red would have more carbon if conditions had remained the same as the first decade while regions that are blue would have less.

Future circulation changes

Depth-integrated velocity fields are first calculated by time-averaging within each future projection period (2015-2042, 2043-2070, and 2071-2098), and then compared against that during the historical period (1981-2014), in order to investigate the future circulation changes in response to the high-emission scenario (Figure 7). We found that the future currents on the outer shelf move offshore, as indicated by the intensities inshore lower in the future, but higher near the slope. The inshore coastal current in the Gulf of Maine also intensifies. This is consistent with prior projections [Clark et al. 2022] with the same model domain, but different downscaling methods. In general, the surface circulation changes are larger in magnitude than the depth-integrated.

Future rates of change

The surface and the bottom trends continue to differ in the future and most of the rates accelerate into the future under SSP5-8.5 (Figure 8, and supplemental Figures S18, and S19). In general, the trends are more severe at the bottom than at the surface in the MAB for both Ω and pH when compared over the entire simulation (1980-2098; Figure 8, and supplemental Figures S18, and S19). The range of variability experienced for Ω is reduced in the future (Figure 8; S18; S19). This is consistent with the increased TA projected in addition to the trends in DIC, T, and S. Further north, they are more comparable for Ω or more severe at the surface, but more severe at the bottom for pH (Figure 8). The DIC trends are more severe subsurface than at the surface (Figure S18) while TA is the opposite (Figure S18). Deoxygenation is more severe on the Scotian Shelf and the MAB than in the GOM (Figure S19). These trends combined with the temperature and salinity patterns latitudinally (cooler in the north) contribute to the spatial pattern of the simulated trends.

Nearly all the rates of change accelerate into the future under SSP5-8.5, but the spatial patterns of the trends shift as well. DIC trends increase by a factor of 2, increasing from nearly 16 μmol/kg/decade to over 32 μmol/kg/decade by the end of the century under this extreme emission scenario. DIC rates of change increase most intensely at the bottom, with faster rates than projected at the surface (Figure 9a; Figure S18). Bottom DIC in Wilkinson Basin increases the slowest in the subsurface environment. Decline in TA slows in the future simulations with declines in TA projected at the surface and bottom of the southern Scotian Shelf, while small increases in TA are found everywhere else (Figure 9b). Interesting patterns emerge along the shelf break of the MAB where a maximum rate of increase is projected coincident with the region where the outer shelf currents moving offshore.

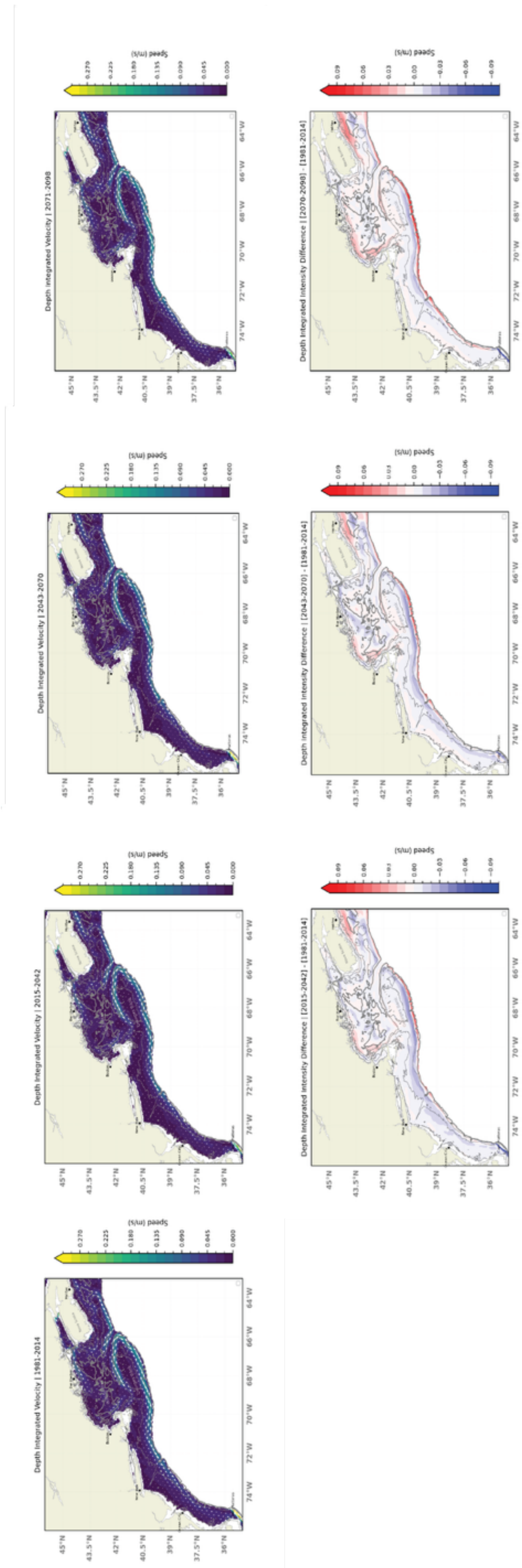
Depth Integrated Velocity | 1981-2014
Depth Integrated Velocity | 2015-2042
Depth Integrated Velocity | 2043-2070
Depth Integrated Velocity | 2071-2098
Depth Integrated Intensity Difference | [2015-2042] - [1981-2014]
Depth Integrated Intensity Difference | [2043-2070] - [1981-2014]
Depth Integrated Intensity Difference | [2070-2098] - [1981-2014]
Speed (m/s)

Figure 7: Maps of the circulation changes from 1981 to 2098 as depth integrated conditions on the NWA shelf. The far left panel show the mean conditions for the entire historical simulation while the three future time periods are showcased on the right three panels. The bottom row showcases the anomalies from historical conditions. Arrow indicate intensity as well as direction of the currents, while colors only indicate intensity.

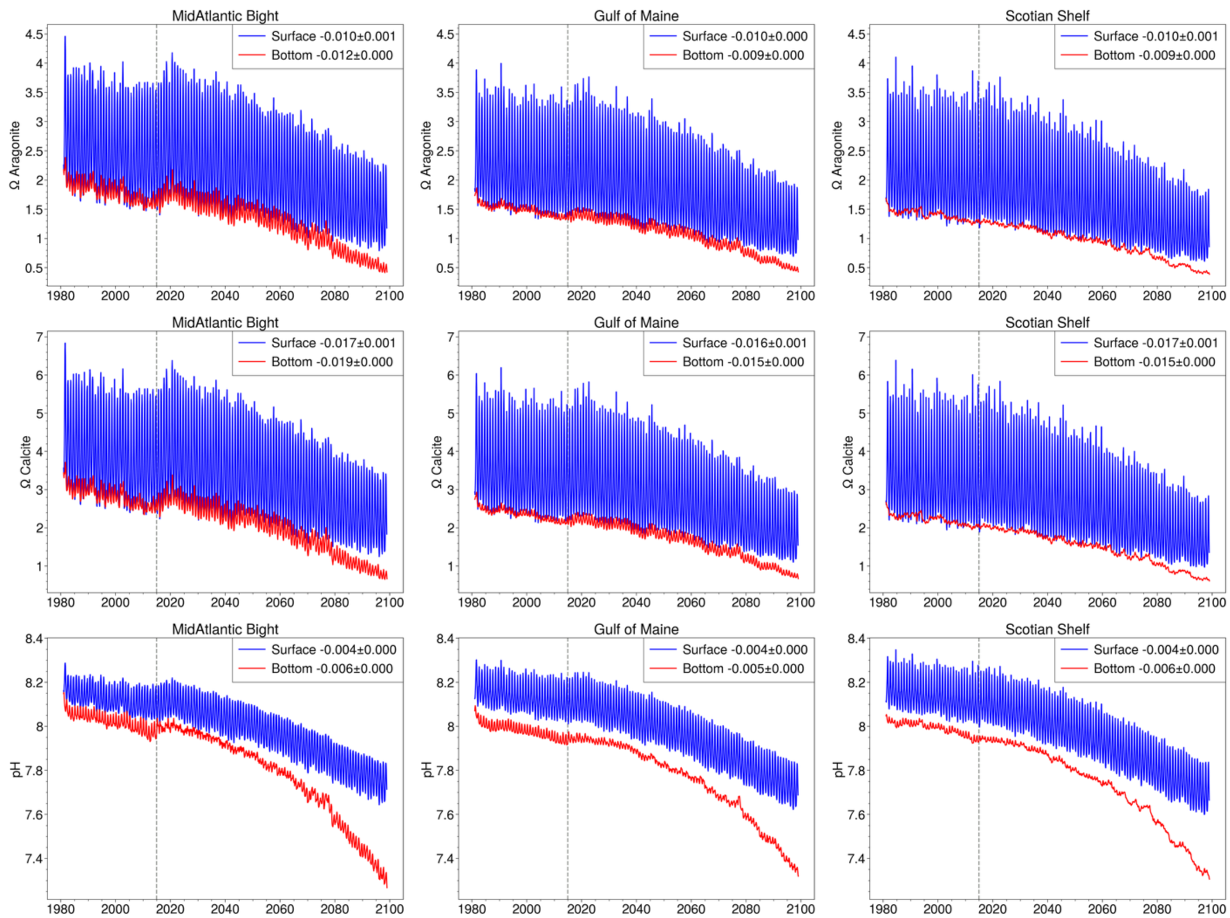

Figure 8: Monthly averaged regional trends from the surface (blue) and bottom (red) spanning the historical simulation (1980-2014, the dashed vertical line) through the future projection under SSP5-8.5 (2015-2098). The top row depicts the trends for Ω_{arag}, the middle row depicts $\Omega_{calcite}$, and the bottom row pH. The left column are from the Mid-Atlantic Bight. The middle row are from the Gulf of Maine, and the right column are from the Scotian Shelf. The rates of change (per year) for each time series over the entire record (1980 to 2098) are the values provided in the legend. Additional variables are similarly plotted and can be found in the supplement (Figures S18 and S19).

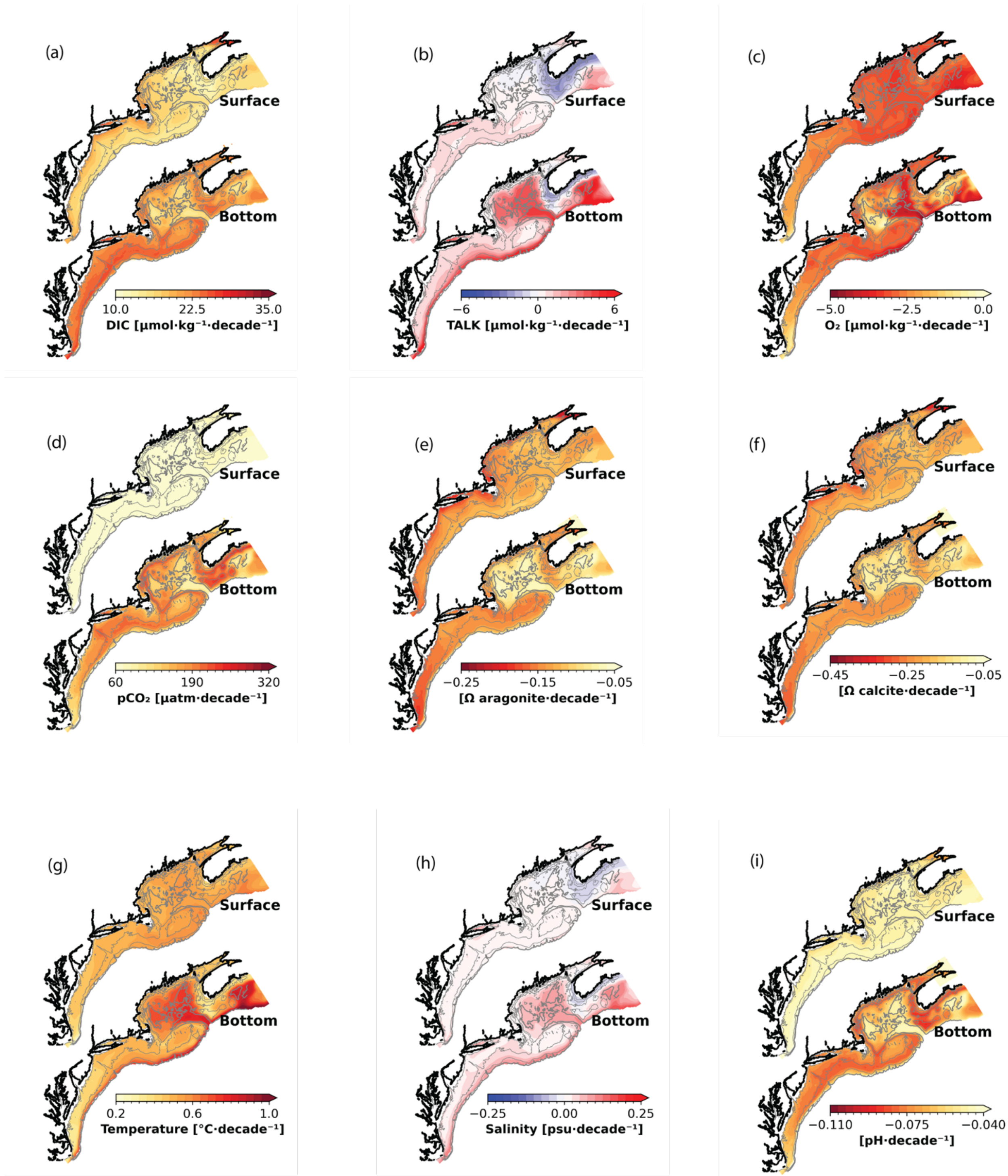

Figure 9: Maps of trends over 2015-2098 of surface and bottom conditions on the NWA shelf within the model domain. (a) DIC, (μmol/kg/decade), (b) TA (μmol/kg/decade), (c) oxygen (μmol/kg/decade), (d) pCO_2 (μatm/decade), (e) Ω_{arag}, (f) $\Omega_{calcite}$, (g) temperature (deg C/decade), (h) salinity (psu/decade), (i) pH on the total scale (per decade)

Oxygen decline accelerates in the future, in other words, the rate of projected change increases everywhere (Figure 9c; Figure S19). Areas that were increasing historically all change to declining oxygen concentrations in the future. Some regions experience minimal change, like the nearshore side of Georges Bank in Wilkinson Basin, but these regions were already experiencing low oxygen concentrations so the rate of decline could not increase that much. pCO_2 and Ω both accelerate subsurface in the future projections (Figures 9e,f).

Discussion:

Compound change— that is, multiple stressors changing in concert or closely - including warming, salinity changes, deoxygenation, and increasing anthropogenic carbon content—produces distinct regional changes and is driving unique trends over the NWA shelf. Coastal modification of large-scale climate signals has been assessed and identified in other systems [Howard et al., 2020; Siedlecki et al. 2021a; Pilcher et al., 2022; 2025] with very different regional processes responsible for the modification. The overall trends in DIC on the NWA coast are also coastally modified relative to the anthropogenic carbon contribution, meaning despite the addition of anthropogenic carbon altering the DIC content on the shelf, AOU is significantly contributing to rates of DIC change in the region. Notably, on the NWA shelf, hotspots like Wilkinson Basin and Hudson Canyon show amplified trends in DIC due to both anthropogenic carbon accumulation and biological drivers like AOU. Regions with the largest pCO_2 increase were associated with the highest changes in AOU: Hudson Canyon and Wilkinson Basin.

The interpretation as to the driver of the modification component of the compound change differs when considering an individual stressor as opposed to the multiple stressors. For example, oxygen is also declining on the NWA shelf, and the trend is driven in large part by AOU despite observed rapid warming [Nguyen et al., *in review*]. The AOU trend is driven in part by circulation shifts but is largely unexplained from observations alone [Nguyen et al., *in review*] suggesting more local ecosystem metabolism drivers. Declines in subsurface nutrient concentrations since 2010 have been observed on the Scotian Shelf and are likely driven by a density-related shift in the Gulf

Stream source water toward a less dense, lower-nutrient Gulf Stream contribution [Lehmann et al. 2023]. These local drivers are difficult to diagnose with oxygen alone, but with nutrients, temperature, salinity, and carbon together or compound change, the mechanisms become clearer.

Circulation changes are also causing a change in AOU [Nguyen et al., in review; Claret et al., 2018], which in turn is amplifying the rate of DIC change in some regions like Wilkinson Basin and around Hudson Canyon. Consistent with other climate drivers in the region, the trends in oxygen and DIC seem to be influenced by the large decadal variations in circulation [Nguyen et al., in review; Goncalvez-Neto 2021; Jutras et al., 2020; Gilbert et al., 2005; Claret et al., 2018]. Waters on the shelf are known to oscillate between cooler, fresher Labrador Slope Water, which has lower-nutrient concentrations as well as lower AOU, and warmer, saltier Warm Slope Water, which has higher-nutrient concentrations and higher AOU [Jutras et al., 2020; Townsend et al. 2015, 2023]. These oscillations in water masses can coincide with decadal oscillations like the North Atlantic Oscillation (NAO). For example, the Labrador Current extends further to the south during a low (negative) NAO period driving low nutrient conditions in bottom waters of the Scotian Shelf and vice versa (Petrie & Drinkwater, 1993). Circulation, however, only explains 44% of the trends in the region [Nguyen et al. *in review*]. Despite that, these large decadal oscillations make trend analysis in the region challenging, even with a 30-year record, and may require longer simulations to fully diagnose.

These patterns and mechanisms differ from those on the west coast of the US, for example, and those differences will be discussed more below. All these trends are expected to accelerate in the future under the most severe emissions scenario explored with projections here. The different magnitudes of amplification in the surface and at the bottom persist making observation strategies for observing this change imperative.

Patterns and estimates of anthropogenic carbon on shelves

Here we estimated anthropogenic carbon inventory accumulated over the NWA shelf between 1998 and 2014 and can now compare this estimate to other shelves and estimates for the NWA (23-35 μmol kg^{-1}). Anthropogenic carbon content for the MAB shelf has been estimated from observations (12-26 μmol kg^{-1} from 1996 to 2018; Li et al., 2024). Li et al. (2024) also found that DIC had increased over the entire water column in the MAB over this time interval. They suggest that most of the anthropogenic carbon is not stored locally on the shelf but rather exported to the open ocean thus contributing to the NWA shelf's well-established status as a sink for atmospheric CO_2 [Laruelle et al., 2010; Regnier et al., 2022; 2013; Roobaert et al., 2024]. This concept is consistent with our differences between the total DIC trends over the simulated time period and the estimated anthropogenic carbon accumulated over this period, including the tendency for the MAB shelf to have a declining DIC trend without the addition of anthropogenic carbon (Figure 5). Water mass changes in the region likely influence the presence of anthropogenic carbon in the region, which is why the water mass approach was adopted by Li et al. (2024). Gulf Stream water is rich in anthropogenic carbon [Cai et al., 2020; Wanninkhof et al., 2015], while estuarine waters were assumed to be poor or in fact contain no anthropogenic carbon in Li et al. (2024). Li et al. (2024) justify this approach because freshwater often has high pCO_2 already, a short residence time, and low buffering capacity. Notably observations of freshwaters in the region are known to contain lower DIC than offshore waters in the region [Salisbury et al. 2009; Gomez et al. 2023]. This assumption differs from our approach and likely contributes to our higher estimate of anthropogenic carbon for the region. Li et al. (2024) point out in their supplementary materials that this choice does influence the total accumulation, and our assumptions would be more consistent with the delta DIC method described there, which results in the highest estimates of anthropogenic carbon accumulation. Our approach allows for surface waters to equilibrate with the atmosphere, which the Li et al. (2024) work assumes is not possible as the residence time of fresher waters is too short in the system. Finally, Li et al. (2024) do not allow for the properties in the end members (e.g. Laurentian Current, Gulf Stream) to change over time, and we know that surface waters in the North Atlantic have increasing contributions of anthropogenic carbon from observations due to rising atmospheric concentrations [Santana-Toscano et al. 2025].

Historically, the simulated DIC_{anthro} (30 μmol /kg) contributes ~0.4 units of the total 0.6 units of the overall decline in Ω_{arag}. If the observed estimate of Li et al. (2024) is used, that contribution is reduced. Determining the contribution of anthropogenic carbon contributions from estuaries and rivers in the region is important to refine to better constrain this quantity in the NWA region. Despite these differences, both estimates agree that the anthropogenic carbon inventory is still lower than estimates from the west coast of the US [Feely et al., 2024].

On the west coast of the US, Feely et al. (2024) estimates between 15-80 μmol/kg of anthropogenic carbon reside in shelf waters with greater concentrations near the surface, in the southern California Current System, and lower values observed subsurface [Feely et al., 2024, 2016]. On the east coast of the US, higher anthropogenic carbon values are observed in the subsurface and on the outer shelf [Li et al., 2024], but simulated inventories here suggest shallow waters and consistently higher in anthropogenic carbon with secondary highs located on the outer coast. Notably, the shelf and coastal processes differ drastically from those on the east coast of the US [McGarry et al., 2021], including relevant processes to carbon cycling [Cai et al., 2020]. Offshore source waters have higher anthropogenic waters in the North Atlantic than in the Pacific [Carter et al., 2021], contributing to the spatial differences between the regions. Additionally, waters are warmer and fresher on the NWA shelf contributing to lower carbon inventories [Cai et al., 2020]. These regional process-based differences have important implications for both the future as well as observing regional change, highlighting the importance of observing and understanding the hot spots for change on the NWA shelf.

Drivers of differences between surface and bottom trends – modification mechanisms

Surface trends differ from bottom trends in both the historical and future simulations with the bottom trends simulated to be more intense. This pattern has been observed in an analysis of historical warming rates in the region using temperature observations previously [Friedland et al., 2020]. Friedland et al. (2020) identified different warming change points between the surface and bottom observations. They suggested more atmospheric drivers at the surface and more advective controls at the subsurface as one possible explanation for these trends. Consistent with this, surface temperatures experience a larger seasonal variation than bottom temperature or salinity does [Richaud et al., 2016].

Biogeochemically, surface atmospheric drivers of changes in carbon would likely follow changes in atmospheric conditions, while advective driven changes in carbon variables would be mirrored in patterns for AOU as well as T and S changes. Our results are indeed consistent with that pattern, with the largest AOU trends coinciding with the largest bottom DIC changes (Figure 5), while the surface trends are largely the same as the atmospheric trends (Figure 3d, ~12-19 μatm/decade).

A recent analysis in Roobaert et al. (2024) of global coastal trends in carbon fluxes reveals that the long-term trend of the air–sea pCO_2 gradient drives most of the long-term evolution of the coastal CO_2 sink, wind speed and sea-ice coverage playing a significant role regionally. In the NWA, our simulated surface and bottom trend patterns are consistent with the mechanisms responsible for the difference between the physical drivers described by Friedland et al. (2020) and Roobaert et al. (2024) with some refinement. On the NWA shelf, Roobaert et al. (2024) identify the region as primarily a sink for CO_2 despite what recent observations have suggested based on in situ observations in the region [Sutton et al., 2016; Xu et al., 2020]. This conclusion, that the region is a net sink for carbon, is also consistent with the recent multi-decadal analysis performed by Li et al. (2024), which also identifies export from the shelf to the open ocean as an important process to better understand and simulate.

There are two locations where AOU changes are identified as being critically important for amplifying local DIC changes, shaping benthic trends: Wilkinson Basin and Hudson Canyon. Wilkinson Basin has long been identified as a region of older recirculated waters [Pringle 2006; Runge et al., 2014; Townsend et al., 2015]. The region surrounding Hudson Canyon has only recently emerged as a potential hot spot for OA in the Ecosystem Status report from the NEFSC produced by NOAA annually [NEFSC 2023]. AOU can be driven by circulation shifts, ventilation changes, or changes in local biological processes like respiration of organic material [Kwiatkowski et al., 2020; Long et al., 2019; Schmidtko et al., 2017; Takano et al., 2018], both of which are occurring in these regions. More work is needed to identify the cause of AOU in this region locally and determine the relative importance of circulation and local biological processes to controlling the trends in this region into the future, but the simulated biogeochemical trend differences between the surface and bottom environments identified here support the physical controls on the differences in surface and bottom trends in the region. Consistent with this, in the regions further north off of Canada, Gibb et al. (2022) demonstrates clear links between the physical environment and the carbonate system along their Atlantic shelves as well. In the future projections, the differences between the surface and the bottom trends continues but accelerates relative to the historical rates.

Implications for Observing Trends:

Downscaled climate models require long term observations to evaluate these important feedbacks in models and ensure the trends are achieved for the right reasons including regional process-based feedback. Surface trends have been established in the MAB region [Xu et al., 2020] and in the GOM [Salisbury and Jonsson 2018] by reconstructing observations using empirically based statical methods. Our trends reported here (Figure 3) compare well with observed trends reported in both works, with the notable exception of total alkalinity trends, which appear more uncertain. In the MAB, Xu et al. (2020) reconstructed surface trends spanning 1982 to 2015 and found that the shelf water DIC content was increasing at a rate of 10.6 +/- 2.2 μmol/kg per decade, which compares well with our simulated regional trends (Figure 3a). TA was reported as increasing slightly (3.3 +/- 3.9 μmol/kg per decade) but notably the uncertainty range was large, suggesting the direction of the change was uncertain. Further north, on the Scotian Shelf, simulations [Mei et al, 2024] and observations [Lehmann et al. 2023] indicate freshening is occurring in that region, and the Labrador Current is known to be freshening due to freshening in the Arctic Ocean as well [Zhang et al. 2021]. Our simulation identifies a decline in TA in surface waters of the region (Figure 3b) but is also known to be biased fresh. This could represent a water mass bias in our simulations on the shelf or imply some missing important carbonate feedback in our underlying assumptions as all the works used empirical reconstruction approaches. The difference is also potentially due to the disagreement in the salinity fields as well as each work uses different salinity products.

Reconstructions rely on the strong relationship between salinity and TA observed in the ocean [Lee et al., 2006], but that approach leaves errors larger (RMSE of 11 μmol/kg, Salisbury and Jonsson 2018) than the trends reported in any of these works despite strong correlations observed between these quantities. The strong disagreement in our approaches suggests more work is needed to refine our understanding of TA trends in the region.

A decline of 0.103 +/-0.010 per decade was observed for Ω_{arag} while in the GOM Salisbury and Jonsson (2018) report a decline of 0.049 +/- 0.009 per decade between 1981 and 2014. Our simulation suggests a similar range of rates of decline in surface waters of the region including the spatial patterns with MAB experiencing a more severe trend in surface waters (Figure 3e). In the NWA region, the frequency of observing to capture the modeled trends suggests that annual observations every summer are necessary for carbon variables (not shown). Typically, NOAA OAP ECOA cruises occur every 3-5 years currently, but other NOAA cruises do measure some basic hydrography and carbon variables seasonally (e.g. ECOMON and LTER). In addition, bottom conditions in the GOM change a few years before the surface temperatures [Balch et al., 2022] with important implications for observing this trend. So benthic conditions are likely to influence surface conditions years later for biogeochemistry as well. By prioritizing benthic observations in the region, surface field simulations and forecasts will likely also be improved.

The time period of the observations used to quantify trends matters because of the large decadal variation observed in this region [Nguyen et al., *in review;* Salisbury and Jonsson, 2018]. When computing the trends, the trends may look different depending on the time window within which are computed [Sutton et al., 2022], which is why multiple decades of simulation or observations is recommended [Drenkard et al., 2021]. In the NWA, a significant shift occurred in the mid 2010s, which is when our historical simulation ends. This shift may affect the comparisons with other estimated trends observed in the region. Notably, Salisbury and Jonsson (2018) suggested that the surface Ω was increasing in the GOM between 2006 and 2014, as did [Xu et al., 2020] for the MAB, which they refer to as a hiatus in the decline. Salisbury and. Jonsson (2018) examined a 34-

year record (1981-2014) within which only 5-10 years of anomaly perturbed the regional carbon system. Over the longer term, the decline of pH was evident, but short-term variability sometimes caused the direction of change to reverse for Ω, in particular. They noted the significant role of decadal variation for Ω trends, which also shows up in our simulation.

Conclusions:

Observing this compound change requires not only over-constraint on the carbon cycle parameters, but also multiple co-existing biogeochemical observations to refine the mechanisms responsible for local climate variability. Surface and bottom water rates of change differ for carbon variables on the NWA shelf historically and these trends accelerate into the future. The overall trends in DIC on this coast are modified including the anthropogenic carbon contribution, meaning both circulation changes and AOU are contributing to rates and patterns of DIC content change in the region. Historically, the DIC_{anthro} (30 μmol /kg) contributes ~0.4 units of change to the overall decline in Ω_{arag}. These modified patterns continue in the future simulations. Downscaled projections continue to be necessary to simulate compound changes in coastal regions.

Data Statement:

The climatological historical conditions can be found here:
Samantha Siedlecki, et al. (2025). Model fields supporting the publication " Understanding historical and projected compound change on the Northwest Atlantic shelf “- historical climatology [Data set]. Submitted to *Progress in Oceanography*. Zenodo. 10.5281/zenodo.16421224

The climatological future conditions can be found here:
Samantha Siedlecki, et al. (2025). Model fields supporting the publication " Understanding historical and projected compound change on the Northwest Atlantic shelf “- future climatology [Data set]. Submitted to *Progress in Oceanography*. Zenodo. 10.5281/zenodo.16422060

Research Data:

Observations from the region were obtained through a series of publicly available databases including NCEI and World Ocean Database. A compilation of the raw model data supporting the conclusions of this article will be made available by the authors upon request, without undue reservation. The figures were generated using Python.

Funding sources:

This work was supported by NOAA's Ocean Acidification program [NA20OAR0170475, NA19OAR0170351]; NOAA's Climate Program Office [NA21OAR4310120-T1-01]; and NSF's convergence accelerator.

Supplement

See separate file currently included below.

Author Contributions:

Samantha Siedlecki: Conceptualization, Methodology, Investigation, Funding acquisition, Project administration, Supervision, Resources, **Felipe Soares.**: Data curation, Software, Formal analysis, Visualization, Writing- Reviewing and Editing. **Zhuomin Chen**: Formal analysis, Visualization, Writing- Reviewing and Editing. **Enrique Curchitser**: Software, Writing- Reviewing and Editing, Funding acquisition. **Hung Nguyen:** Formal analysis, Writing- Reviewing and Editing, Visualization. **Shannon Meseck:** Writing- Reviewing and Editing, Funding acquisition. **Michael Alexander:** Writing- Reviewing and Editing, Funding acquisition, Methodology. **S Shin:** Writing- Reviewing and Editing, Formal analysis, Methodology. **Catherine Matassa:** Writing- Reviewing and Editing, Funding acquisition. **Halle Berger:** Writing- Reviewing and Editing, Visualization

Competing Interests

The authors declare that they have no conflict of interest.

Acknowledgements:

We would like to acknowledge conversations with Joe Salisbury and Charlie Stock as helpful to formulating our thinking for this work. We would also like to extend our gratitude to the individuals at NOAA for providing a constructive internal review.

References cited

Alexander, M. A., Shin, S., Scott, J. D., Curchitser, E., Stock, C. (2019) The Response of the Northwest Atlantic Ocean to Climate Change. *J. Climate*, submitted.

Allen, J., P. Somerfield, and F. Gilbert (2007), Quantifying uncertainty in high-resolution coupled hydrodynamic-ecosystem models, *J. Mar. Syst.*,64(1–4), 3–14, doi:10.1016/j.jmarsys.2006.02.010.

Andersen, S., Grefsrud, E. S., Harboe, T. (2013). Effect of increased pCO2 level on early shell development in great scallop (Pecten maximus Lamarck) larvae. *Biogeosciences*, *10*, 6161-6184. https://doi.org/10.5194/bg-10-6161-2013.

Anderson, R., Rowe, G.T., Kemp, P.F., Trumbore, S., Biscaye P.E. (1994). Carbon budget for the mid-slope depocenter of the Middle Atlantic Bight. *Deep-Sea Research II 41(2/3)*, 669-703.

Balch, W.M., Drapeau, D.T., Bowler, B.C., Record, N.R., Bates, N.R., Pinkham, S., Garley, R. and Mitchell, C., (2022). Changing hydrographic, biogeochemical, and acidification properties in the Gulf of Maine as measured by the Gulf of Maine North Atlantic Time Series, GNATS, between 1998 and 2018. *Journal of Geophysical Research: Biogeosciences*, 127(6), p.e2022JG006790.

Beardsley, R. C., Winant, C. D. (1979). On the Mean Circulation in the Mid-Atlantic Bight. *Journal of Physical Oceanography 9*.

Bopp, L., Resplandy, L., Orr, J., Doney, S., Dunne, J., Gehlen, M., Vichi, M. (2013). Multiple stressors of ocean ecosystems in the 21st century: Projections with CMIP5 models. *Biogeosciences 10*. https://doi.org/10.5194/bg-10-6225-2013

Boyer, T.P., O.K. Baranova, C. Coleman, H.E. Garcia, A. Grodsky, R.A. Locarnini, A.V. Mishonov, C.R. Paver, J.R. Reagan, D. Seidov, I.V. Smolyar, K. Weathers, M.M. Zweng,(2018): World Ocean Database 2018. A.V. Mishonov, Technical Ed., NOAA Atlas NESDIS 87.

Breitburg, D., Levin, L. A., Oschlies, A., Grégoire, M., Chavez, F. P., Conley, D. J., Zhang, J. (2018). Declining oxygen in the global ocean and coastal waters. *Science*, *359*(6371). https://doi.org/10.1126/science.aam7240

Brickman, D, et al. (2021). Projections of physical conditions in the Gulf of Maine in 2050. *Elem Sci Anth*, 9: 1. DOI: https://doi.org/ 10.1525/elementa.2020.20.00055

Cai, W. J., Hu, X., Huang, W. J., Jiang, L. Q., Wang, Y., Peng, T. H., Zhang, X. (2010). Alkalinity distribution in the western North Atlantic Ocean margins. *Journal of Geophysical Research: Oceans*. https://doi.org/10.1029/2009JC005482

Cai, W. J., Hu, X., Huang, W. J., Murrell, M. C., Lehrter, J. C., Lohrenz, S. E., Gong, G. C. (2011). Acidification of subsurface coastal waters enhanced by eutrophication. *Nature Geoscience*. https://doi.org/10.1038/ngeo1297

Cai, WJ., Xu, YY., Feely, R.A. et al. Controls on surface water carbonate chemistry along North American ocean margins. *Nat Commun* 11, 2691 (2020). https://doi.org/10.1038/s41467-020-16530-z

Carter, B.R., Feely, R.A., Lauvset, S.K., Olsen, A., DeVries, T. and Sonnerup, R., (2021). Preformed properties for marine organic matter and carbonate mineral cycling quantification. *Global Biogeochemical Cycles*, 35(1), p.e2020GB006623.

Chang, J.-H., Hart, D. R., Munroe, D. M., & Curchitser, E. N. (2021). Bias correction of ocean bottom temperature and salinity simulations from a regional circulation model using regression kriging. *Journal of Geophysical Research: Oceans*, 126(4), e2020JC017140. https://doi.org/10.1029/2020JC017140

Chapman, D. C., Barth, J. A., Beardsley, R. C., Fairbanks, R. G. (1986). On the Continuity of Mean Flow between the Scotian Shelf and the Middle Atlantic Bight. *Journal of Physical Oceanography*, *16*(4), 758–772. https://doi.org/10.1175/1520-0485

Chapman, D. C., Beardsley, R. C. (1989). On the Origin of Shelf Water in the Middle Atlantic Bight. *Journal of Physical Oceanography 19*.384-391.

Chen, K., He, R., Powell, B. S., Gawarkiewicz, G. G., Moore, A. M., Arango, H. G. (2014). Data assimilative modeling investigation of Gulf Stream Warm Core Ring interaction with continental shelf and slope circulation. *Journal of Geophysical Research C: Oceans*. https://doi.org/10.1002/2014JC009898

Chen, Z., & Curchitser, E. N. (2020). Interannual variability of the Mid-Atlantic bight cold pool. *Journal of Geophysical Research: Oceans*, 125(8), e2020JC016445. https://doi.org/10.1029/2020jc016445

Chen, Z., Curchitser, E., Chant, R., Kang, D. (2018). Seasonal Variability of the Cold Pool Over the Mid-Atlantic Bight Continental Shelf. *Journal of Geophysical Research: Oceans*, *123*(11), 8203–8226. https://doi.org/10.1029/2018JC014148

Christensen, P., K. Gillingham, & W. Nordhaus, Uncertainty in forecasts of long-run economic growth, *Proc. Natl. Acad. Sci.* U.S.A. 115 (21) 5409-5414, https://doi.org/10.1073/pnas.1713628115 (2018).

Claret, M., Galbraith, E., Palter, J., Bianchi, D., Fennel, K., Gilbert, D., Dunne, J. (2018). Rapid coastal deoxygenation due to ocean circulation shift in the northwest Atlantic. *Nature Climate Change8*. https://doi.org/10.1038/s41558-018-0263-1

Clark, S., Hubbard, K.A., Ralston, D.K., McGillicuddy, D.J., Stock, C., Alexander, M.A., and E. Curchitser (2022). Projected effects of climate change on Pseudonitzschia bloom dynamics in the Gulf of Maine. *Journal of Marine Systems*. https://doi.org/10.1016/j.jmarsys.2022.103737

Cooley, S. R., Doney, S. C. (2009). Anticipating ocean acidification's economic consequences for commercial fisheries. *Environmental Research Letters*. https://doi.org/10.1088/1748-9326/4/2/024007

Dai, A., T. Qian, and K. E. Trenberth. (2009). Changes in continental freshwater discharge from 1948 to 2004. *J.Climate*, 22, 2773–2792, doi:10.1175/2008JCLI2592.1.

De Vries, P., Döös, K. (2001). *Calculating Lagrangian Trajectories Using Time-Dependent Velocity Fields*. *Journal of Atmospheric and Oceanic Technology - J ATMOS OCEAN TECHNOL18.* https://doi.org/10.1175/1520-0426

Dee, D. P., S. M. Uppala, A. J. Simmons, P. Berrisford, P. Poli, S. Kobayashi, U. Andrae, et al. (2011). "The ERA-Interim Reanalysis: Configuration and Performance of the Data Assimilation System." *Quarterly Journal of the Royal Meteorological Society*137 (656): 553–97. https://doi.org/10.1002/qj.828.

Deser C, Knutti R, Solomon S, Phillips AS (2012) Communication of the role of natural variability in future North American climate. *Nat Clim Change* 2(11):775–779. doi:10.1038/nclimate1562

Deser C, Phillips AS, Alexander MA, Smoliak BV (2014) Projecting North American Climate over the next 50 years: Uncertainty due to Internal Variability. *J. Climate*, 27, 2271–2296, https://doi.org/10.1175/JCLI-D-13-00451.1.

Deutsch, C., Berelson, W., Thunell, R., Weber, T., Tems, C., McManus, J., van Geen, A. (2014). Centennial changes in North Pacific anoxia linked to tropical trade winds. *Science*,*345*(6197), 665–668. https://doi.org/10.1126/science.1252332

Diaz, R. J., Rosenberg, R. (2008). Spreading Dead Zones and Consequences for Marine Ecosystems. *Science*,*321*(5891), 926–929. https://doi.org/10.1126/science.1156401

Doney, S. C. (2010). The growing human footprint on coastal and open-Ocean biogeochemistry. *Science*. https://doi.org/10.1126/science.1185198

Döös, K. (2012). TRACMASS Lagrangian Trajectory Code Documentation and Manual. In: http://www.tracmass.org/. 45.

Döös, K., Nilsson, J., Nycander, J., Brodeau, L., Ballarotta, M. (2012). The World ocean thermohaline circulation.*Journal of Physical Oceanography*. doi: 10.1175/JPO-D-1111-0163.1171.

Döös, K., Rupolo, V., Brodeau, L. (2011). Dispersion of surface drifters and model-simulated trajectories. *Ocean Modelling 39*, 301-310, doi:310.1016/j.ocemod.2011.1005.1005.

Dorman, J.G., Castruccio, F.S., Curchitser, E.N., Kleypas, J.A., Powell, T.M. (2016). Modeled connectivity of Acropora millepora populations from reefs of the Spratly Islands and the greater South China Sea. *Coral Reefs 35*, 169-179.

Drenkard, E. J., Stock, C., Ross, A. C., Dixon, K. W., Adcroft, A., Alexander, M., Balaji, V., Bograd, S. J., Butenschön, M., Cheng, W., Curchitser, E., Lorenzo, E.

D., Dussin, R., Haynie, A. C., Harrison, M., Hermann, A., Hollowed, A., Holsman, K., Holt, J., Jacox, M. G., Jang, C. J., Kearney, K. A., Muhling, B. A., Buil, M. P., Saba, V., Sandø, A. B., Tommasi, D., and Wang, M. (2021) Next-generation regional ocean projections for living marine resource management in a changing climate. *ICES Journal of Marine Science*, 0:1-19.

Dunne, J. P., John, J. G., Shevliakova, E., Stouffer, R. J., Krasting, J. P., Malyshev, S. L., Zadeh, N. (2012). GFDL's ESM2 Global Coupled Climate–Carbon Earth System Models. Part II: Carbon System Formulation and Baseline Simulation Characteristics. *Journal of Climate*, *26*(7), 2247–2267. https://doi.org/10.1175/JCLI-D-12-00150.1

du Pontavice, H. and Chen, Z. and Saba, V.S. (2023). "A high-resolution ocean bottom temperature product for the northeast U.S. continental shelf marine ecosystem". *Progress in Oceanography*. Vol. 210. https://doi.org/10.1016/j.pocean.2022.102948

Eyring, V., Bony, S., Meehl, G. A., Senior, C. A., Stevens, B., Stouffer, R. J., Taylor, K. E. (2016). Overview of the Coupled Model Intercomparison Project Phase 6 (CMIP6) experimental design and organization. *Geoscientific Model Development*, *9*(5), 1937–1958. https://doi.org/10.5194/gmd-9-1937-2016

Feely RA, Alin SR, Carter B, Bednaršek N, Hales B. (2016). Chemical and biological impacts of ocean acidification along the west coast of North America. *Estuar. Coast. Shelf Sci* 183A:260–70

Feely, R. A., Carter, B. R., Alin, S. R., Greeley, D., and Bednaršek, N. (2024). The combined effects of ocean acidification and respiration on habitat suitability for marine calcifiers along the west coast of North America, *J. Geophys. Res.-Oceans*, 129, e2023JC019892, https://doi.org/10.1029/2023JC019892.

Feely, R. A., Okazaki, R. R., Cai, W. J., Bednaršek, N., Alin, S. R., Byrne, R. H., Fassbender, A. (2018). The combined effects of acidification and hypoxia on pH and aragonite saturation in the coastal waters of the California current ecosystem and the northern Gulf of Mexico. *Continental Shelf Research*. https://doi.org/10.1016/j.csr.2017.11.002

Feely, R. A., Sabine, C. L., Hernandez-Ayon, J. M., Ianson, D., Hales, B. (2008). Evidence for upwelling of corrosive "acidified" water onto the continental shelf. *Science*. https://doi.org/10.1126/science.1155676

Fennel, K., Wilkin, J., Levin, J., Moisan, J., O'Reilly, J., Haidvogel, D. (2006). Nitrogen cycling in the Middle Atlantic Bight: Results from a three-dimensional model and implications for the North Atlantic nitrogen budget. *Global Biogeochemical Cycles*, *20*(3). https://doi.org/10.1029/2005GB002456

Fennel, K., Wilkin, J., Previdi, M., Najjar, R. (2008). Denitrification effects on air-sea CO2 flux in the coastal ocean: Simulations for the northwest North Atlantic. *Geophysical Research Letters*, *35*(24), 1–5. https://doi.org/10.1029/2008GL036147

Fratantoni, P. S., Pickart, R. S. (2007). The Western North Atlantic Shelfbreak Current System in Summer. *Journal of Physical Oceanography*, *37*(10), 2509–2533. https://doi.org/10.1175/JPO3123.1

Friedland KD, Morse RE, Manning JP, et al. (2020). Trends and change points in surface and bottom thermal environments of the US Northeast Continental Shelf Ecosystem. *Fish Oceanog*raphy, 29, 396–414. https://doi.org/10.1111/fog.12485

Fryxell, J. M., Packer, C., McCann, K., Solberg, E. J., Sæther, B. E. (2010). Resource management cycles and the sustainability of harvested wildlife populations. *Science*. https://doi.org/10.1126/science.1185802

Gattuso, J.-P., Magnan, A., Billé, R., Cheung, W. W. L., Howes, E. L., Joos, F., Turley, C. (2015). Contrasting futures for ocean and society from different anthropogenic CO2 emissions scenarios. *Science*, 349(6243), aac4722. https://doi.org/10.1126/science.aac4722

Gibb, O., Cyr, F., Azetsu-Scott, K., Chassé, J., Childs, D., Gabriel, C.-E., Galbraith, P. S., Maillet, G., Pepin, P., Punshon, S., and Starr, M., (2023). Spatiotemporal variability in pH and carbonate parameters on the Canadian Atlantic continental shelf between 2014 and 2022, *Earth Syst. Sci. Data*, 15, 4127–4162, https://doi.org/10.5194/essd-15-4127-2023

Gilbert, D., Sundby, B., Gobeil, C., Mucci, A. and Tremblay, G.H., (2005). A seventy-two-year record of diminishing deep-water oxygen in the St. Lawrence estuary: The northwest Atlantic connection. *Limnology and oceanography*, 50(5), pp.1654-1666.

Gledhill, D., White, M., Salisbury, J., Thomas, H., Misna, I., Liebman, M., Doney, S. (2015). Ocean and Coastal Acidification off New England and Nova Scotia. *Oceanography*, *28*. https://doi.org/10.5670/oceanog.2015.41

Gomez, F. A., Lee, S.-K., Stock, C. A., Ross, A. C., Resplandy, L., Siedlecki, S. A., Tagklis, F., and Salisbury, J. E. (2023). RC4USCoast: a river chemistry dataset for regional ocean model applications in the US East Coast, Gulf of Mexico, and US West Coast, *Earth Syst. Sci. Data*, 15, 2223–2234, https://doi.org/10.5194/essd-15-2223-2023.

Gonçalves Neto, A., Langan, J.A. & Palter, J.B. (2021). Changes in the Gulf Stream preceded rapid warming of the Northwest Atlantic Shelf. *Commun Earth Environ* 2, 74. https://doi.org/10.1038/s43247-021-00143-5

Gonçalves Neto, A., Palter, J. B., Xu,X., & Fratantoni, P. (2023). Temporalvariability of the Labrador Currentpathways around the tail of the GrandBanks at intermediate depths in ahigh-resolution ocean circulation model. *Journal of Geophysical Research:Oceans*, 128, e2022JC018756. https://doi.org/10.1029/2022JC018756

Grogan, D. S. (2016). Global and Regional Assessments of Unsustainable Groundwater Use in Irrigated Agriculture. Doctoral Dissertations. 2260. https://scholars.unh.edu/dissertation/2260

Gruber, N., Frenzel, H., Doney, S. C., Marchesiello, P., McWilliams, J. C., Moisan, J. R., Stolzenbach, K. D. (2006). Eddy-resolving simulation of plankton ecosystem dynamics in the California Current System. *Deep Sea Research Part I: Oceanographic Research Papers*, *53*(9), 1483–1516. https://doi.org/10.1016/j.dsr.2006.06.005

Hales, B., Emerson, S. (1997). Evidence in support of first-order dissolution kinetics of calcite in seawater. *Earth and Planetary Science Letters 148(1-2):317-327* https://doi.org/10.1016/S0012-821X(97)00017-4

Hare, J. A., Cowen, R. K. (2009). Transport Mechanisms of Larval and Pelagic Juvenile Bluefish (Pomatomus saltatrix) from South Atlantic Bight Spawning Grounds to Middle Atlantic Bight Nursery Habitats. *American Society* 41(6), 1264–1280.

Hare JA, Morrison WE, Nelson MW, Stachura MM, Teeters EJ, Griffis RB, Alexander MA, Scott JD, Alade L, Bell RJ, Chute AS, Curti KL, Curtis TH, Kircheis D, Kocik JF, Lucey SM, McCandless CT, Milke LM, Richardson DE, Robillard E, Walsh HJ, McManus MC, Marancik KE, Griswold CA. (2016). A Vulnerability Assessment of Fish and Invertebrates to Climate Change on the Northeast U.S. Continental Shelf. *PLoS One.* Feb 3;11(2):e0146756. doi: 10.1371/journal.pone.0146756. PMID: 26839967; PMCID: PMC4739546.

Hartmann, D. L., Klein Tank, A. M. G., Rusticucci, M., Alexander, L. V., Brönnimann, S., Charabi, Y. A. R., Zhai, P. (2013). Observations: Atmosphere and surface. *Climate Change 2013 the Physical Science Basis: Working Group I Contribution to the Fifth Assessment Report of the Intergovernmental Panel on Climate Change*. https://doi.org/10.1017/CBO9781107415324.008

Hawkins E, Sutton R (2009) The potential to narrow uncertainty in regional climate predictions. Bull Am Meteorol Soc 90(8):1095–1107. doi:10.1175/2009BAMS2607.1

Houghton, R. W., Schlitz, R., Beardsley, R. C., Butman, B., Chamberlin, J. L. (1982). The Middle Atlantic Bight Cold Pool: Evolution of the Temperature Structure During Summer 1979. *Journal of Physical Oceanography*, *12*(10), 1019–1029. https://doi.org/10.1175/1520-0485

Howard, E. M., Frenzel, H., Kessouri, F., Renault, L., Bianchi, D., McWilliams, J. C., & Deutsch, C. (2020). Attributing causes of future climate change in the California Current System with multi-model downscaling *Global Biogeochemical Cycles*, 34, e2020GB006646, https://doi.org/10.1029/2020GB006646.

Huang, T.-H., Cai, W.-J., Vlahos, P., Wallace, D. W. R., Lewis, E. R., & Chen, C.-T. A. (2021). The mid-Atlantic Bight dissolved inorganic carbon system observed in the March 1996 DOE Ocean Margins Program (OMP)—A baseline study. *Frontiers in Marine Science*, 8(June), 1–16. https://doi.org/10.3389/fmars.2021.629412

Hunt, C., Salisbury, J., Vandemark, D. (2011). Contribution of non-carbonate anions to total alkalinity and overestimation of pCO2 in New England and New Brunswick rivers. *Biogeosciences*. https://doi.org/10.5194/bg-8-3069-2011

Hausfather, Z. & Peters, G. Emissions – the 'business as usual' story is misleading. *Nature* 577, 618–620 (2020).

Ito, T., Minobe, S., Long, M.C. and Deutsch, C., (2017). Upper ocean O2 trends: 1958–2015. *Geophysical Research Letters*, 44(9), pp.4214-4223

Jahnke R., Richards, M., Nelson, J., Robertson, C., Rao, A., Jahnke, D. (2005). Organic matter remineralization and porewater exchange rates in permeable South Atlantic Bight continental shelf sediments. *Continental Shelf Research 25,* 1433–1452.

Jiang, L.-Q., Feely, R. A., Wanninkhof, R., Greeley, D., Barbero, L., Alin, S., Carter, B. R., Pierrot, D., Featherstone, C., Hooper, J., Melrose, C., Monacci, N., Sharp, J. D., Shellito, S., Xu, Y.-Y., Kozyr, A., Byrne, R. H., Cai, W.-J., Cross, J., Johnson, G. C., Hales, B., Langdon, C., Mathis, J., Salisbury, J., and Townsend, D. W. (2021). Coastal Ocean Data Analysis Product in North America (CODAP-NA) – an internally consistent data product for discrete inorganic carbon, oxygen, and nutrients on the North American ocean margins, *Earth Syst. Sci. Data*, 13, 2777–2799, https://doi.org/10.5194/essd-13-2777-2021.

Jiang LQ, Feely RA, Carter BR, Greeley DJ, Gledhill DK, Arzayus KM. (2015). Climatological distribution of aragonite saturation state in the global oceans. *Glob. Biogeochem. Cycles* 29:1656–73. https://doi.org/10.1002/2015GB005198

Jönsson B., Döös K., Myrberg K., Lundberg P.A. (2011). A Lagrangian-trajectory study of a gradually mixed estuary. *Continental Shelf Research 31*, 1811-1817.

Joyce, T. M., Bishop, J. K. B., Brown, O. B. (1992). Observations of offshore shelf-water transport induced by a warm-core ring. *Deep-Sea Research.39*, S97--S113.

Jutras, M., Dufour, C. O., Mucci, A., Cyr, F. & Gilbert, D. (2020). Temporal changes in the causes of the observed oxygen decline in the St. Lawrence Estuary. J. Geophys. Research: Oceans 125, e2020JC016577.

Jutras, M., Dufour, C. O., Mucci, A., & Talbot, L. C. (2023). Large-scale control of the retroflection of the Labrador Current. *Nature Communications*, *14*(1), Article 1. https://doi.org/10.1038/s41467-023-38321-y

Kang, D., Curchitser, E. N. (2013). Gulf Stream eddy characteristics in a high-resolution ocean model. *Journal of Geophysical Research: Oceans*, *118*(9), 4474–4487. https://doi.org/10.1002/jgrc.20318

Kessouri, F., McLaughlin, K., Sutula, M., Bianchi, D., Ho, M., McWilliams, J.C., Renault, L., Molemaker, J., Deutsch, C. and Leinweber, A., (2021). Configuration and validation of an oceanic physical and biogeochemical model to investigate coastal eutrophication in the Southern California Bight. *Journal of Advances in Modeling Earth Systems*, 13(12), p.e2020MS002296.

Kim, S. Y., Kosro, P. M. (2013). Observations of near-inertial surface currents off Oregon: Decorrelation time and length scales. *Journal of Geophysical Research: Oceans*, *118*(7), 3723–3736. https://doi.org/10.1002/jgrc.20235

Kriegler, E; Bauer, N; Popp, A; Humpenoeder, F; Leimbach, M; Strefler, J; Baumstark, L; Bodirsky, BL; Hilaire, J; Klein, D; Mouratiadou, I; Weindl, I; Bertram, C; Dietrich, JanP; Luderer, G; Pehl, M; Pietzcker, R; Piontek, F; Lotze-Campen, H; Biewald, A; Bonsch, M; Giannousakis, A; Kreidenweis, U; Mueller, C; Rolinski, S; Schultes, A; Schwanitz, J; Stevanovic, M; Calvin, K; Emmerling, J; Fujimori, S; Edenhofer, O (2021). Fossil-fueled development (SSP5): An energy and resource intensive scenario for the 21st century. *Global Environmental Change*. ISSN: 0959-3780. Vol. 42. DOI 10.1016/j.gloenvcha.2016.05.015

Kwiatkowski, L., Torres, O., Bopp, L., Aumont, O., Chamberlain, M., Christian, J. R., et al. (2020). Twenty-first century ocean warming, acidification, deoxygenation, and upper-ocean nutrient and primary production decline from CMIP6 model projections. *Biogeosciences*, 17(13), 3439–3470. https://doi.org/10.5194/bg-17-3439-2020

Lammers, R. B., Shiklomanov, A. I., Vörösmarty, C. J., Fekete, B. M., Peterson, B. J. (2001). Assessment of contemporary Arctic river runoff based on observational discharge records. *Journal of Geophysical Research: Atmospheres*, *106*(D4), 3321–3334. https://doi.org/10.1029/2000JD900444

Laruelle, G. G., Cai, W. J., Hu, X., Gruber, N., Mackenzie, F. T., Regnier, P. (2018). Continental shelves as a variable but increasing global sink for atmospheric carbon dioxide. *Nature Communications*. https://doi.org/10.1038/s41467-017-02738-z

Laruelle, G. G., Dürr, H. H., Slomp, C. P., and Borges, A. V. (2010). Evaluation of sinks and sources of CO2 in the global coastal ocean using a spatially explicit typology of estuaries and continental shelves, *Geophys. Res. Lett*., 37, L15607, https://doi.org/10.1029/2010GL043691.

Lee, K., Tong, L. T., Millero, F. J., Sabine, C. L., Dickson, A. G., Goyet, C., Park, G.-H., Wanninkhof, R., Feely, R. A., and Key, R. M. (2006). Global relationships of total alkalinity with salinity and temperature in surface waters of the world's oceans, *Geophys. Res. Lett.*, 33, L19605, https://doi.org/10.1029/2006GL027207, 2006.

Le Quéré, C., Andrew, R. M., Friedlingstein, P., Sitch, S., Pongratz, J., Manning, A. C., Zhu, D. (2018). Global Carbon Budget 2018. *Earth System Science Data*. https://doi.org/10.5194/essd-10-405-2018

Lehner, B., Liermann, C. R., Revenga, C., Vörösmarty, C., Fekete, B., Crouzet, P., Wisser, D. (2011). High-resolution mapping of the world's reservoirs and dams for sustainable river-flow management. *Frontiers in Ecology and the Environment*, *9*(9), 494–502. https://doi.org/10.1890/100125

Lentz, S. J. (2008). Observations and a Model of the Mean Circulation over the Middle Atlantic Bight Continental Shelf. *Journal of Physical Oceanography*. https://doi.org/10.1175/2007jpo3768.1

Li, X., Wu, Z., Ouyang, Z., Cai, W. (2024). The source and accumulation of anthropogenic carbon in the U.S. East Coast. *Science Advances* .10, eadl3169(2024). DOI:10.1126/sciadv.adl3169

Lima, F. P., Wethey, D. S. (2012). Three decades of high-resolution coastal sea surface temperatures reveal more than warming. *Nature Communications*. https://doi.org/10.1038/ncomms1713

Liu, J., Hertel, T. W., Lammers, R. B., Prusevich, A., Baldos, U. L. C., Grogan, D. S., Frolking, S. (2017). Achieving sustainable irrigation water withdrawals: global impacts on food security and land use. *Environmental Research Letters*, *12*(10), 104009. https://doi.org/10.1088/1748-9326/aa88db

Loder, J. W., B. Petrie, and G. Gawarkiewicz, (1998). The coastal ocean off northeastern North America: A large-scale view. The Sea: The Global Coastal Ocean, Vol. 11, Regional Studies and Syntheses, A. R. Robinson and K. H. Brink, Eds., Wiley, 105–133.

Long, M. C., Ito, T., & Deutsch, C. (2019). Ocean deoxygenation: Everyone's problem. Causes, impacts, consequences and solutions. In D. Laffoley, & J. M. Baxter (Eds.), Ocean deoxygenation: Everyone's problem. Causes, impacts, consequences and solutions. (pp. 263–268). IUCN, International Union for Conservation of Nature. https://doi.org/10.2305/IUCN.CH.2019.13.en

Maréchal, D. (2004). A Soil-Based Approach to Rainfall-Runoff Modelling in Ungaugaed Catchments for England and Wales, PhD Thesis, Cranfield University. 157 pp.

McDougall, T.J. and P.M. Barker. (2011). Getting started with TEOS-10 and the Gibbs Seawater (GSW) Oceanographic Toolbox, 28pp., SCOR/IAPSO WG127, ISBN 978-0-646-55621-5.

McGarry, K., S.A. Siedlecki, J. Salisbury, and S. R. Alin. (2021). Multiple linear regression models for reconstructing and exploring processes controlling the carbonate system of the northeast US from basic hydrographic data. *JGR-Oceans*, 126, e2020JC016480. https://doi.org/10.1029/2020JC016480

Mei Z-P, Lavoie D, Lambert N, Starr M, Chassé J, Perrie W and Long Z (2024) Modelling the bottom-up effects of climate change on primary production in the Gulf of St. Lawrence and eastern Scotian Shelf. Front. Mar. Sci. 11:1416744. doi: 10.3389/fmars.2024.1416744

Menzel, D. W., States., U. (1993). Ocean processes: U.S. southeast continental shelf: a summary of research conducted in the South Atlantic Bight under the auspices of the U.S. Department of Energy from 1977 to 1991. Oak Ridge, TN: U.S. Dept. of Energy, Office of Scientific and Technical Information. file://catalog.hathitrust.org/Record/007198953

Mills, K.E., A.J. Pershing, C.J. Brown, Y. Chen, F.-S. Chiang, D.S. Holland, S. Lehuta, J.A. Nye, J.C. Sun, A.C. Thomas, and R.A. Wahle. (2013). Fisheries management in a changing climate: Lessons from the 2012 ocean heat wave in the Northwest Atlantic. *Oceanography* 26(2):191–195, https://doi.org/10.5670/oceanog.2013.27.

Northeast Fisheries Science Center (U.S.) "State of the Ecosystem 2023: Mid-Atlantic" (2023), https://doi.org/10.25923/vy6j-w454

National Marine Fisheries Service. (2018). Fisheries of the United States, 2017. U.S. Department of Commerce, NOAA Current Fishery Statistics No. 2017 Available at: https://www.fisheries.noaa.gov/feature-story/ fisheries-united-states-2017

Nguyen, H.**, Siedlecki, S.A. et al. (in review). Temporal Trends of Deoxygenation in the Northwest Atlantic Ocean: an observational approach. *JGR-Oceans*

Nye, J. A., Joyce, T. M., Kwon, Y.-O., Link, J. S. (2011). Silver hake tracks changes in Northwest Atlantic circulation. *Nature Communications*, *2*, 412. https://doi.org/10.1038/ncomms1420

O'Neill, B. C., Tebaldi, C., van Vuuren, D. P., Eyring, V., Friedlingstein, P., Hurtt, G., Sanderson, B. M. (2016). The Scenario Model Intercomparison Project (ScenarioMIP) for CMIP6. *Geoscientific Model Development*, *9*(9), 3461–3482. https://doi.org/10.5194/gmd-9-3461-2016

Packer, D., M. Cargnelli, L., J. Griesbach, S., Shumway, S. (1999). Essential Fish Habitat Source Document: Sea Scallop, Placopecten magellanicus, Life History and Habitat Characteristics.*NOAA Tech Memo NMFS NE 134*.

Perez, Fiz F, Marcos Fontela, Maribel I García-Ibáñez, Herlé Mercier, Anton Velo, Pascale Lherminier, Patricia Zunino, et al. (2018). "Meridional Overturning Circulation Conveys Fast Acidification to the Deep Atlantic Ocean." *Nature* 554 (February): 515. https://doi.org/10.1038/nature25493.

Pershing AJ, Alexander MA, Hernandez CM, Kerr LA, Le Bris A, Mills KE, Nye JA, Record NR, Scannell HA, Scott JD, Sherwood GD, Thomas AC. (2015). Slow adaptation in the face of rapid warming leads to collapse of the Gulf of Maine cod fishery. *Science*. Nov 13;350(6262):809-12. doi: 10.1126/science.aac9819. Epub 2015 Oct 29. PMID: 26516197.

Petrie, B., & Drinkwater, K. (1993). Temperature and salinity variability on the Scotian Shelf and in the Gulf of Maine 1945–1990. *Journal of Geophysical Research*, 98(C11), 20079–20089. https://doi.org/10.1029/93JC02191

Pilcher, D. J., Cross, J. N., Monacci, N., Mu, L., Kearney, K. A., Hermann, A. J., and Cheng, W. (2025). Amplified bottom water acidification rates on the Bering Sea shelf from 1970–2022, *Biogeosciences*, 22, 3103–3125, https://doi.org/10.5194/bg-22-3103-2025.

Pilcher, D.J., Cross, J.N., Hermann, A.J., Kearney, K.A., Cheng, W. and Mathis, J.T., (2022). Dynamically downscaled projections of ocean acidification for the

Bering Sea. *Deep Sea Research Part II: Topical Studies in Oceanography*, 198, p.105055.

Pilcher, D. J., Siedlecki, S. A., Hermann, A. J., Coyle, K. O., Mathis, J. T., Evans, W. (2018). Simulated Impact of Glacial Runoff on CO2 Uptake in the Gulf of Alaska. *Geophysical Research Letters*. https://doi.org/10.1002/2017GL075910

Pomeroy, L. R., Sheldon, J. E., Sheldon, W. M., Blanton, J. O., Amft, J., Peters, F. (2000). Seasonal changes in microbial processes in estuarine and continental shelf waters of the South-eastern U.S.A. *Estuarine, Coastal and Shelf Science*, *51*(4), 415–428. https://doi.org/10.1006/ecss.2000.0690

Pozo Buil, M., Jacox, M. G., Fiechter, J., Alexander, M. A., Bograd, S. J., Curchitser, E. N., et al. (2021). A dynamically downscaled ensemble of future projections for the California current system. *Frontiers in Marine Science*, 8. https://doi.org/10.3389/fmars.2021.612874

Pringle JM. (2006). Sources of variability in Gulf of Maine circulation, and the observations needed to model it. *Deep Sea Res* 53(23–24):2457–2476. https://doi.org/10.1016/j.dsr2.2006.08.015

Qi, D., Chen, L., Chen, B., Gao, Z., Zhong, W., Feely, R. A., Cai, W. J. (2017). Increase in acidifying water in the western Arctic Ocean. *Nature Climate Change*. https://doi.org/10.1038/nclimate3228

Rabalais, N. N., Diaz, R. J., Levin, L. A., Turner, R. E., Gilbert, D., Zhang, J. (2010). Dynamics and distribution of natural and human-caused hypoxia. *Biogeosciences*, *7*(2), 585–619.

Raymond, P. A., Cole, J. J. (2003). Increase in the Export of Alkalinity from North America's Largest River. *Science*, *301*(5629), 88–91. https://doi.org/10.1126/science.1083788

Regnier, P., Friedlingstein, P., Ciais, P., Mackenzie, F.T., Gruber, N., Janssens, I.A., Laruelle, G.G., Lauerwald, R., Luyssaert, S., Andersson, A.J. and Arndt, S., (2013). Anthropogenic perturbation of the carbon fluxes from land to ocean. *Nature geoscience*, 6(8), pp.597-607.

Regnier, P., Resplandy, L., Najjar, R.G. et al. (2022).The land-to-ocean loops of the global carbon cycle. *Nature* 603, 401–410 https://doi.org/10.1038/s41586-021-04339-9

Rennick, M. A. (1977). The Parameterization of Tropospheric Lapse Rates in Terms of Surface Temperature. *Journal of the Atmospheric Sciences*, *34*(6), 854–862. https://doi.org/10.1175/1520-0469

Rheuban, J. E., Doney, S. C., Cooley, S. R., Hart, D. R. (2018). Projected impacts of future climate change, ocean acidification, and management on the US Atlantic sea scallop (Placopecten magellanicus) fishery. *PLoS ONE*, *13*(9), 1–21. https://doi.org/10.1371/journal.pone.0203536

Richaud, B., Kwon, Y. O., Joyce, T. M., Fratantoni, P. S., Lentz, S. J. (2016). Surface and bottom temperature and salinity climatology along the continental shelf off the Canadian and U.S. East Coasts. *Continental Shelf Research*, *124*, 165–181. https://doi.org/10.1016/j.csr.2016.06.005

Roobaert, A., Regnier, P., Landschützer, P., and Laruelle, G. G. (2024). A novel sea surface pCO_2-product for the global coastal ocean resolving trends over 1982–2020, *Earth Syst. Sci. Data*, 16, 421–441, https://doi.org/10.5194/essd-16-421-2024.

Ross, A. C., Stock, C. A., Adcroft, A., Curchitser, E., Hallberg, R., Harrison, M. J., Hedstrom, K., Zadeh, N., Alexander, M., Chen, W., Drenkard, E. J., du Pontavice, H., Dussin, R., Gomez, F., John, J. G., Kang, D., Lavoie, D., Resplandy, L., Roobaert, A., Saba, V., Shin, S.-I., Siedlecki, S., and Simkins, J. (2023). A high-resolution physical–biogeochemical model for marine resource applications in the northwest Atlantic (MOM6-COBALT-NWA12 v1.0), *Geosci. Model Dev.*, 16, 6943–6985, https://doi.org/10.5194/gmd-16-6943-2023.

Rossby, T., Benway, R. L. (2000). Slow variations in mean path of the Gulf Stream east of Cape Hatteras. *Geophysical Research Letters*, *27*(1), 117–120. https://doi.org/10.1029/1999GL002356

Runge, J.A., Ji, R., Thompson, C.R.S., Record, N.R., Chen, C., Vandemark, D.C., Salisbury, J.E., Maps, F. (2014). Persistence of Calanus finmarchicus in the western Gulf of Maine during recent extreme warming, *Journal of Plankton Research*, Volume 37, Issue 1, Pages 221–232, https://doi.org/10.1093/plankt/fbu098

Saba, V. S., Griffies, S. M., Anderson, W. G., Winton, M., Alexander, M. A., Delworth, T. L., Zhang, R. (2016). Enhanced warming of the Northwest Atlantic Ocean under climate change. *Journal of Geophysical Research: Oceans*. https://doi.org/10.1002/2015JC011346

Salisbury, J. E., Jönsson, B. F. (2018). Rapid warming and salinity changes in the Gulf of Maine alter surface ocean carbonate parameters and hide ocean acidification. *Biogeochemistry*. https://doi.org/10.1007/s10533-018-0505-3

Salisbury, J., Vandemark, D., Hunt, C., Campbell, J., Jonsson, B., Mahadevan, A., Xue, H. (2009). Episodic riverine influence on surface DIC in the coastal Gulf of Maine. *Estuarine, Coastal and Shelf Science*. https://doi.org/10.1016/j.ecss.2008.12.021

Sarmiento, J. L., Gruber, N. (2006). *Ocean Biogeochemical Dynamics*. Princeton University Press. http://www.jstor.org/stable/j.ctt3fgxqx

Santana-Toscano, D., Brown, P., & Hernández-Guerra, A. (2025). Anthropogenic carbon dynamics: Concentrations, transports, and trends in the western North Atlantic Subtropical Gyre. *Journal of Geophysical Research: Oceans*, 130, e2025JC022493. https://doi.org/10.1029/2025JC022493

Sarofim, M.C., Smith, C.J., Malek, P. et al. High radiative forcing climate scenario relevance analyzed with a ten-million-member ensemble. *Nat Commun* 15, 8185 (2024). https://doi.org/10.1038/s41467-024-52437-9

Schmidtko, S., Stramma, L., & Visbeck, M. (2017). Decline in global oceanic oxygen content during the past five decades. *Nature*, 542(7641), 335–339. https://doi.org/10.1038/nature21399

Shchepetkin, A. F., McWilliams, J. C. (2005). The regional oceanic modeling system (ROMS): a split-explicit, free-surface, topography-following-coordinate oceanic model. *Ocean Modelling*, *9*(4), 347–404. https://doi.org/https://doi.org/10.1016/j.ocemod.2004.08.002

Shearman, R. K., Lentz, S. J. (2009). Long-Term Sea Surface Temperature Variability along the U.S. East Coast. *Journal of Physical Oceanography*, *40*(5), 1004–1017. https://doi.org/10.1175/2009JPO4300.1

Siedlecki, S. A., Banas, N. S., Davis, K. A., Giddings, S., Hickey, B. M., MacCready, P., Geier, S. (2015). Seasonal and interannual oxygen variability on the Washington and Oregon continental shelves. *Journal of Geophysical Research: Oceans*, 120(2), 608–633. https://doi.org/10.1002/2014JC010254

Siedlecki, S. A., Pilcher, D. J., Hermann, A. J., Coyle, K., Mathis, J. (2017). The Importance of Freshwater to Spatial Variability of Aragonite Saturation State in the Gulf of Alaska. *Journal of Geophysical Research: Oceans*. https://doi.org/10.1002/2017JC012791

Siedlecki, S. A., Pilcher, D., Howard, E. M., Deutsch, C., MacCready, P., Norton, E. L., Frenzel, H., Newton, J., Feely, R. A., Alin, S. R., and Klinger, T. (2021). Coastal processes modify projections of some climate-driven stressors in the California Current System, *Biogeosciences*, 18, 2871–2890, https://doi.org/10.5194/bg-18-2871-2021.

Siedlecki, S.A., Salisbury, J., Gledhill, D.K., Bastidas, C., Meseck, S., McGarry, K., Hunt, C., Alexander, M. Lavoie, D., Wang, Z.A., Scott, J., Brady, D.C., Mlsna, I., Azetsu-Scott, K., Liberti, C.M., Melrose, D.C., White, M.M., Pershing, A., Vandemark, D., Townsend, D.W., Chen, C., Mook, W., Morrison, R. (2021). Projecting ocean acidification impacts for the Gulf of Maine to 2050: New tools and expectations. *Elementa: Science of the Anthropocene* 21 January 2021; 9 (1): 00062. doi: https://doi.org/10.1525/elementa.2020.00062

Soetaert, K., Middelburg, J. J., Herman, P. M. J., Buis, K. (2000). On the coupling of benthic and pelagic biogeochemical models. *Earth-Science Reviews*, *51*(1), 173–201. https://doi.org/https://doi.org/10.1016/S0012-8252(00)00004-0

Steele, P., Bert, T. M. (1998). The Florida blue crab fishery: History, status, and management. *Journal of Shellfish Research,17*(2), 441-449.

Stevens, A.M.., Gobler, C.J. (2018). Interactive effects of acidification, hypoxia, and thermal stress on growth, respiration, and survival of four North Atlantic bivalves. *Marine Ecology Progress Series*, *604*, 143–161. https://www.int-res.com/abstracts/meps/v604/p143-161/

Stock, C. A., Dunne, J. P., John, J. G. (2014). Global-scale carbon and energy flows through the marine planktonic food web: An analysis with a coupled physical-biological model. *Progress in Oceanography*, *120*, 1–28. https://doi.org/10.1016/j.pocean.2013.07.001

Stockhause, M., Matthews, R., Pirani, A., Treguier, A. M., and Yelekci, O.: CMIP6 data documentation and citation in IPCC's Sixth Assessment Report (AR6), EGU General Assembly 2021, online, 19–30 Apr 2021, EGU21-2886, https://doi.org/10.5194/egusphere-egu21-2886, 2021

Sulpis, O., Boudreau, B. P., Mucci, A., Jenkins, C., Trossman, D. S., Arbic, B. K., Key, R. M. (2018). Current CaCO3 dissolution at the seafloor caused by anthropogenic CO2. *Proceedings of the National Academy of Sciences*, *115*(46), 11700–11705. https://doi.org/10.1073/pnas.1804250115

Sulpis, O., Lix, C., Mucci, A., Boudreau, B. P. (2017). Calcite dissolution kinetics at the sediment-water interface in natural seawater. *Marine Chemistry*, *195*, 70–83. https://doi.org/https://doi.org/10.1016/j.marchem.2017.06.005

Sutton, A.J., Battisti, R., Carter, B., Evans, W., Newton, J., Alin, S., Bates, N.R., Cai, W.J., Currie, K., Feely, R.A. and Sabine, C. (2022). Advancing best practices for assessing trends of ocean acidification time series. *Frontiers in Marine Science*, 9, p.1045667.

Sutton, A. J., et al. (2016). Using present-day observations to detect when anthropogenic change forces surface ocean carbonate chemistry outside preindustrial bounds, *Biogeosciences*, 13(17), 5065–5083, doi:10.5194/bg-13-5065-2016.

Tachikawa, T., Kaku, M., Iwasaki, A., Gesch, D. B., Oimoen, M. J., Zhang, Z., Carabajal, C. (2011). *ASTER Global Digital Elevation Model Version 2 - summary of validation results*(2nd ed.). Retrieved from http://pubs.er.usgs.gov/publication/70005960

Talley, Feely, R. A., Sloyan, B. M., Wanninkhof, R., Baringer, M. O., Bullister, J. L., Zhang, J.-Z. (2016). Changes in Ocean Heat, Carbon Content, and Ventilation: A Review of the First Decade of GO-SHIP Global Repeat Hydrography. *Annual Review of Marine Science*. https://doi.org/10.1146/annurev-marine-052915-100829

Taylor, K. E., Stouffer, R. J., Meehl, G. A. (2012). An overview of CMIP5 and the experiment design. *Bulletin of the American Meteorological Society*. https://doi.org/10.1175/BAMS-D-11-00094.1

Tommasi, D., and Coauthors, (2017). Managing living marine resources in a dynamic environment: the role of seasonal to decadal climate forecasts. *Prog. Oceanogr.*, doi: 10.1016/j.pocean.2016.12.011.

Townsend, D. W. W., Thomas, a. C. C., Mayer, L. M. M., Thomas, M. A., Quinlan, J. (2004). Oceanography of the Northwest Atlantic continental shelf. In The Sea: The Global Coastal Ocean: Interdisciplinary Regional Studies and Syntheses.

Townsend, D. W., Pettigrew, N. R., Thomas, M. A., Neary, M. G., McGillicuddy Jr, D. J., O'Donnell, J. (2015). Water Masses and Nutrient Sources to the Gulf of

Maine. *Journal of Marine Research*, 73(3–4), 93–122. https://doi.org/10.1357/002224015815848811

Townsend, D.W., Pettigrew, N.R., Thomas, MA, Moore, S. (2023). Warming waters of the Gulf of Maine: the role of shelf, slope and Gulf Stream water masses *Prog. Oceanogr*., 215 (2023), pp. 1-28, 10.1016/j.pocean.2023.103030

Trumbull, J. V. (1972). Atlantic continental shelf and slope of the United States; sand-size fraction of bottom sediments, New Jersey to Nova Scotia. *Professional Paper*. https://doi.org/10.3133/pp529K

Tsujino, H., Urakawa, S., Nakano, H., Small, R.J., Kim, W.M., Yeager, S.G., Danabasoglu, G., Suzuki, T., Bamber, J.L., Bentsen, M., Böning, C., Bozec, A., Chassignet, E., Curchitser, E., Dias, F.B., Durack, P.J., Griffies, S.M., Harada, Y., Ilicak, M., Josey, S.A., Kobayashi, C., Kobayashi, S., Komuro, Y., Large, W.G., LeSommer, J., Marsland, S.J., Masina, S., Scheinert, M., Tomita, H., Valdivieso, M., Yamazaki, D., (2018). JRA-55 based surface dataset for driving ocean−sea-ice models (JRA55-do). *Ocean Modelling* 130, 79–139. doi:10.1016/j.ocemod.2018.07.002.

Vörösmarty, C. J., Green, P., Salisbury, J., Lammers, R. B. (2000). Global Water Resources: Vulnerability from Climate Change and Population Growth. *Science*, *289*(5477), 284 LP-288. https://doi.org/10.1126/science.289.5477.284

Wang, Z. A., Lawson, G. L., Pilskaln, C. H., Maas, A. E. (2017). Seasonal controls of aragonite saturation states in the Gulf of Maine. *Journal of Geophysical Research: Oceans*, *122*(1), 372–389. https://doi.org/10.1002/2016JC012373

Wang, Z. A., Wanninkhof, R., Cai, W.-J., Byrne, R. H., Hu, X., Peng, T.-H., Huang, W.-J. (2013). The marine inorganic carbon system along the Gulf of Mexico and Atlantic coasts of the United States: Insights from a transregional coastal carbon study. *Limnology and Oceanography*, *58*(1), 325–342. https://doi.org/10.4319/lo.2013.58.1.0325

Wanninkhof, R., Barbero, L., Byrne, R., Cai, W.-J., Huang, W.-J., Zhang, J.-Z., Langdon, C. (2015). Ocean acidification along the Gulf Coast and East Coast of the USA. *Continental Shelf Research*. https://doi.org/10.1016/j.csr.2015.02.008

White, M. M., Mullineaux, L. S., McCorkle, D. C., Cohen, A. L. (2014). Elevated pCO2 exposure during fertilization of the bay scallop Argopecten irradians reduces larval survival but not subsequent shell size. *Marine Ecology Progress Series*, *498*, 173–186. https://doi.org/10.3354/meps10621

Wisser, D., Fekete, B. M., Vörösmarty, C. J., Schumann, A. H. (2010). Reconstructing 20th century global hydrography: a contribution to the Global Terrestrial Network- Hydrology (GTN-H). *Hydrology and Earth System Sciences*, *14*(1), 1–24. https://doi.org/10.5194/hess-14-1-2010

Xu, Y. Y., Cai, W. J., Gao, Y., Wanninkhof, R., Salisbury, J., Chen, B., Hussain, N. (2017). Short-term variability of aragonite saturation state in the central Mid-Atlantic Bight. *Journal of Geophysical Research: Oceans*. https://doi.org/10.1002/2017JC012901

Xu, H., Kim, H.-M., Nye, J. A., Hameed, S. (2015). Impacts of the North Atlantic Oscillation on sea surface temperature on the Northeast US Continental Shelf. *Continental Shelf Research*, 105, 60–66. https://doi.org/https://doi.org/10.1016/j.csr.2015.06.005

Xu, Y.-Y., Cai, W.-J., Wanninkhof, R., Salisbury, J., Reimer, J., & Chen, B. (2020). Long-Term Changes of Carbonate Chemistry Variables Along the North American East Coast. *Journal of Geophysical Research: Oceans*, 125, e2019JC015982. https://doi.org/10.1029/2019JC015982

Zhang J., Weijer W., Steele M., Cheng W., Verma T., Veneziani M. (2021). Labrador Sea freshening linked to Beaufort Gyre freshwater release. Nat. Commun. 12, 1229. doi: 10.1038/s41467-021-21470-3

Zhang, S., Curchitser, E. N., Kang, D., Stock, C. A., Dussin, R. (2018). Impacts of Mesoscale Eddies on the Vertical Nitrate Flux in the Gulf Stream Region. *Journal of Geophysical Research: Oceans*, 123(1), 497–513. https://doi.org/10.1002/2017JC013402

Zhang, S., Stock, C.A., Curchitser, E.N., Dussin, R. (2019). A Numerical Model Analysis of the Mean and Seasonal Nitrogen Budget on the Northeast U.S. Shelf. *Journal of Geophysical Research: Oceans* 124, no. 5 (2019), https://doi.org/10.1029/2018jc014308

Supplemental information:

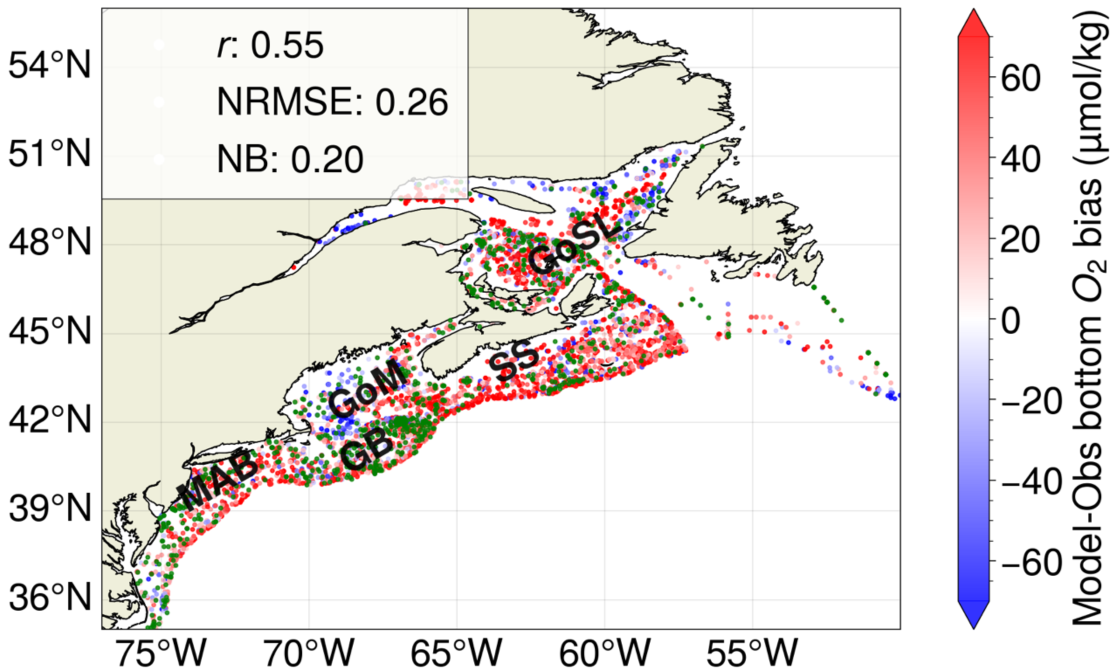

Figure S1: Maps of model evaluation metric bias for oxygen concentrations in µmol/kg compared against the WOD data set for the region between 1980 and 2014. Green values identify regions with minimal bias. Other statistics are reported in the figure as well including the Correlation coefficient (CF), normalized bias(NB), coefficient of determination (R2), relative standard deviation (RSD) with their associated rank (poor = P; good = G; excellent = E).

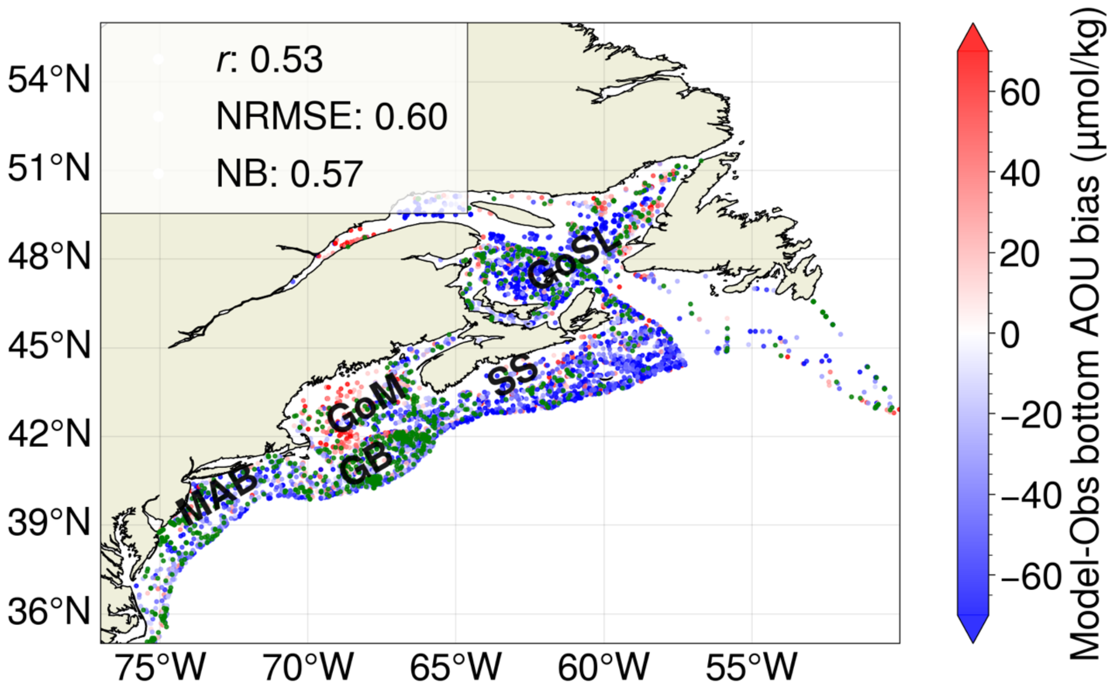

1693
1694

1695 *Figure S2: Maps of model evaluation metric bias for AOU in µmol/kg compared against the*
1696 *WOD data set for the region between 1980 and 2014. Green values identify regions with*
1697 *minimal bias. Other statistics are reported in the figure as well including the Correlation*
1698 *coefficient (CF), normalized bias (NB), coefficient of determination (r), relative standard*
1699 *deviation (RSD) with their associated rank (poor = P; good = G; excellent = E).*

1700

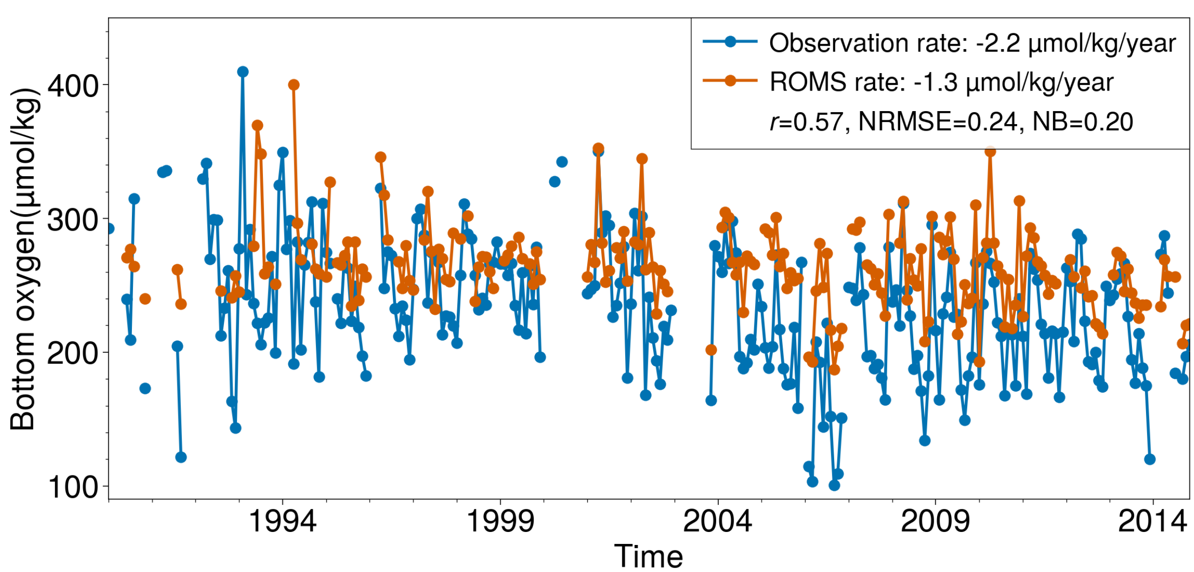

1701

Figure S3: Model evaluation of time series from Nguyen et al (in review) showcasing the regional observed decline in oxygen concentrations in subsurface shelf waters in the NWA region from the WOD data set for the region between 1980 and 2014 from the model (orange) and observations (blue). The observed and modeled rates are reported alongside evaluation metrics: r, NRMSE, NB.

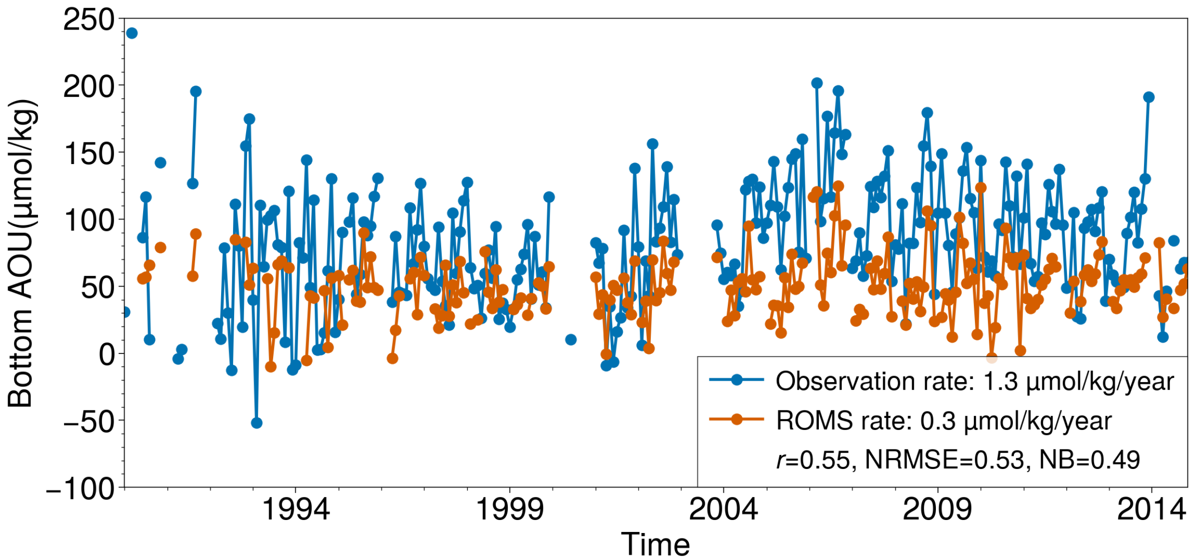

Figure S4: Model evaluation of time series from Nguyen et al (in review) showcasing the regional observed increase in AOU concentrations in subsurface shelf waters in the NWA region from the WOD data set for the region between 1980 and 2014 from the model (orange) and observations (blue). The observed and modeled rates are reported alongside evaluation metrics: r, NRMSE, NB.

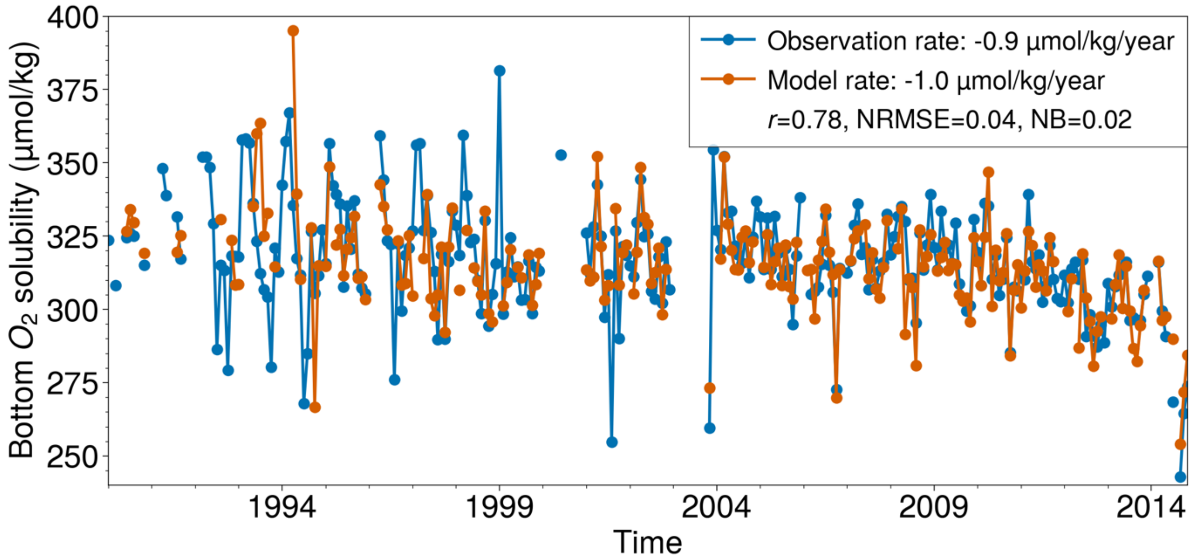

Figure S5: Model evaluation of time series from Nguyen et al (in review) showcasing the regional observed trend in the solubility component of oxygen in shelf waters in the NWA region from the WOD data set for the region between 1980 and 2014 from the model (orange) and observations (blue). The observed and modeled rates are reported alongside evaluation metrics: r, NRMSE, NB.

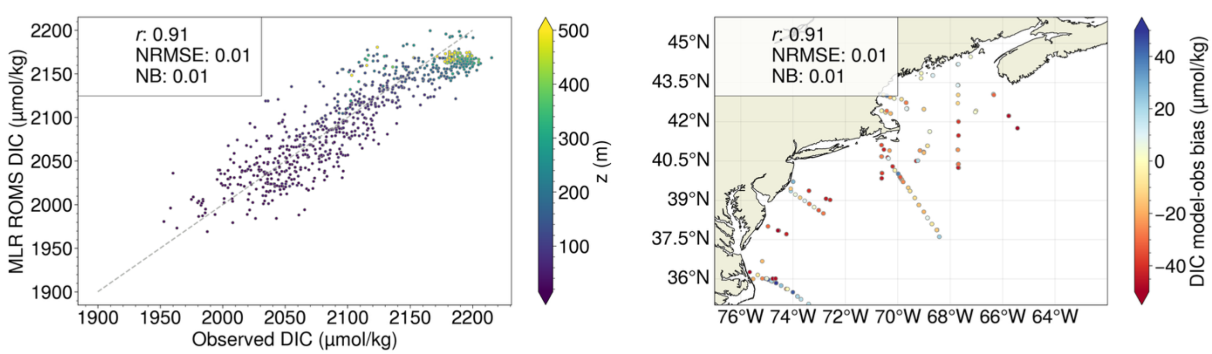

Figure S6: MLR from McGarry et al. (2021) derived DIC comparison between observations and simulations in a scatter plot colored by depth and in a map for bottom waters (right). Model evaluation statistics reported in the inset box of each figure. The observations are retrieved from

CODAP-NA from 2007 to 2014.

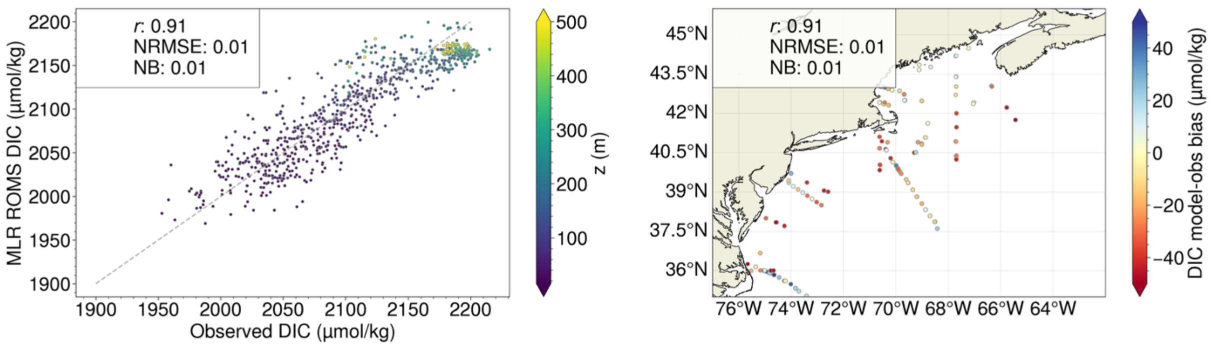

Figure S7: ESPER-NN (Carter et al. 2021) derived DIC comparison between observations and simulations in a scatter plot colored by depth and in a map for bottom waters (right). Model evaluation statistics reported in the inset box of each figure. Observations are retrieved from CODAP-NA from 2007 to 2014.

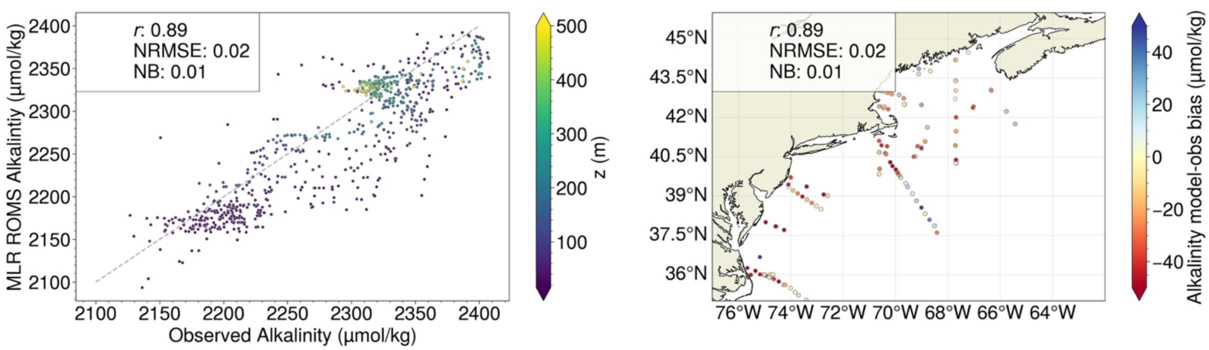

Figure S8: MLR from McGarry et al. (2021) derived TA comparison between observations and simulations in a scatter plot colored by depth and in a map for bottom waters (right). Model evaluation statistics reported in the inset box of each figure. Observations are retrieved from CODAP-NA from 2007 to 2014.

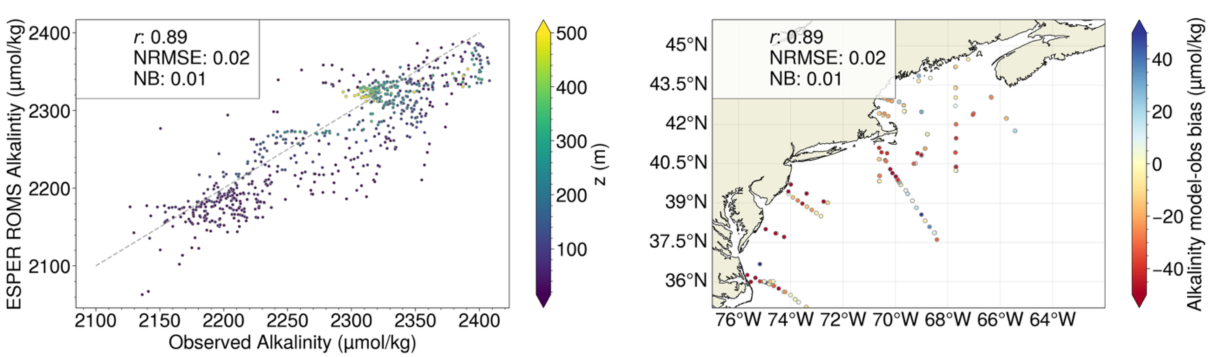

Figure S9: ESPER-NN (Carter et al. 2021) derived TA comparison between observations and simulations in a scatter plot colored by depth and in a map for bottom waters (right). Model evaluation statistics reported in the inset box of each figure. Observations are retrieved from CODAP-NA from 2007 to 2014.

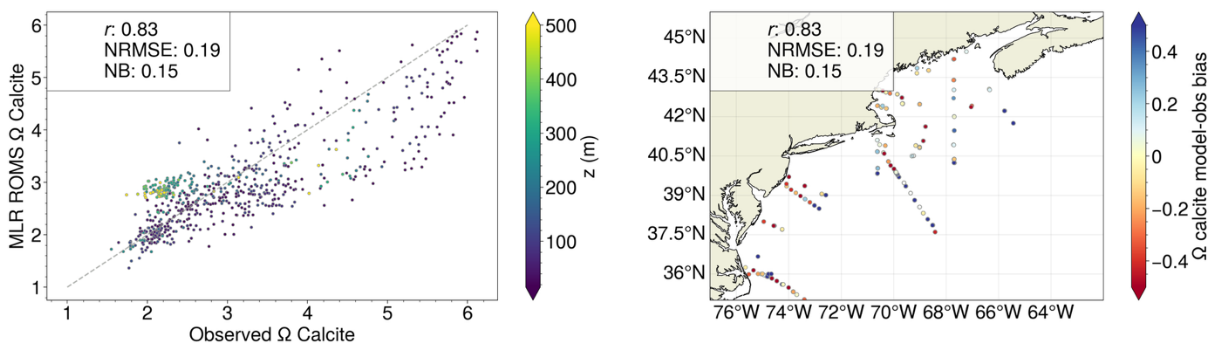

Figure S10: MLR from McGarry et al. (2021) derived $\Omega_{calcite}$ comparison between observations and simulations in a scatter plot colored by depth and in a map for bottom waters (right). Model evaluation statistics reported in the inset box of each figure. The observations are retrieved from CODAP-NA from 2007 to 2014.

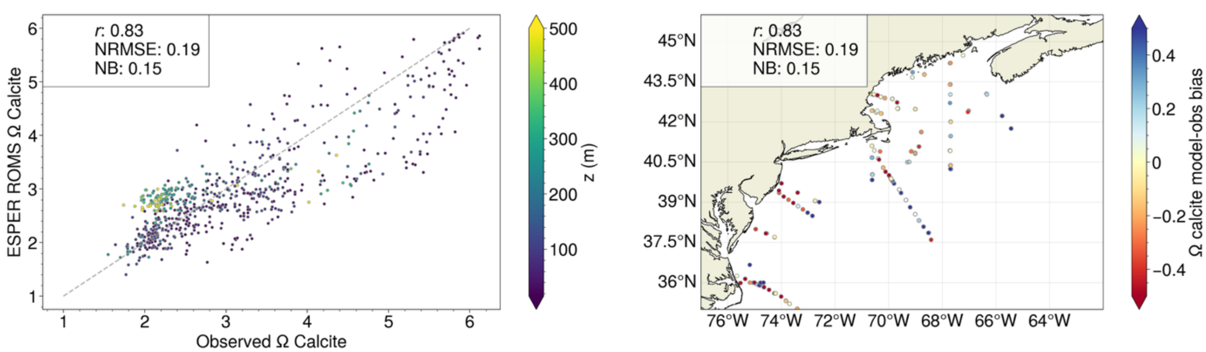

Figure S11: ESPER-NN (Carter et al. 2021) derived $\Omega_{calcite}$ comparison between observations and simulations in a scatter plot colored by depth and in a map for bottom waters (right). Model evaluation statistics reported in the inset box of each figure. Observations are retrieved from CODAP-NA from 2007 to 2014.

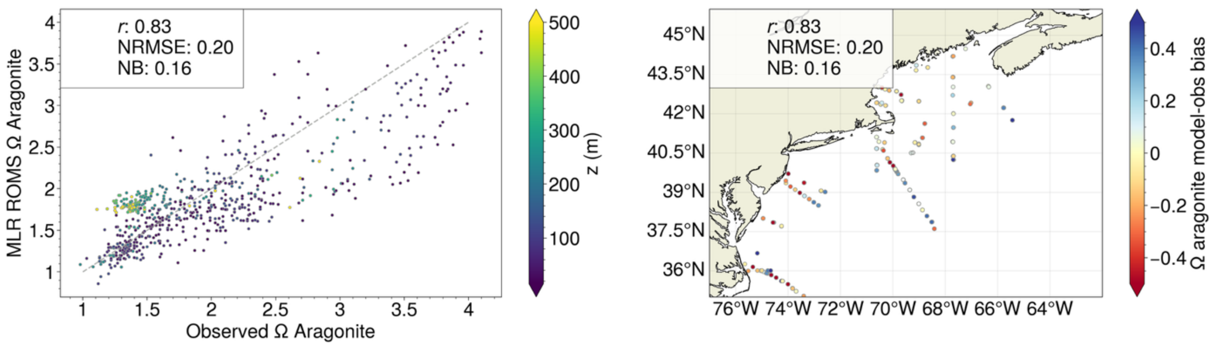

Figure S12: MLR from McGarry et al. (2021) derived Ω_{arag} comparison between observations and simulations in a scatter plot colored by depth and in a map for bottom waters (right). Model evaluation statistics reported in the inset box of each figure. Observations are retrieved from CODAP-NA from 2007 to 2014.

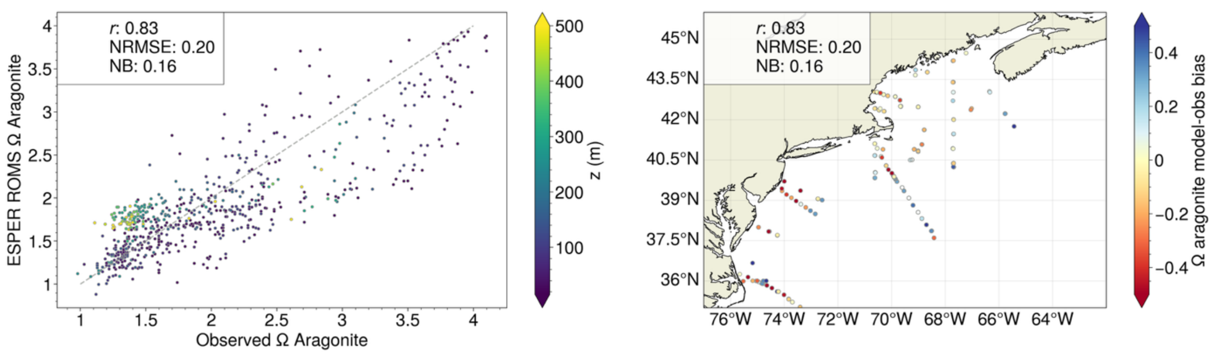

Figure S13: ESPER-NN (Carter et al. 2021) derived Ω_{arag} comparison between observations and simulations in a scatter plot colored by depth and in a map for bottom waters (right). Model evaluation statistics reported in the inset box of each figure. Observations are retrieved from CODAP-NA from 2007 to 2014.

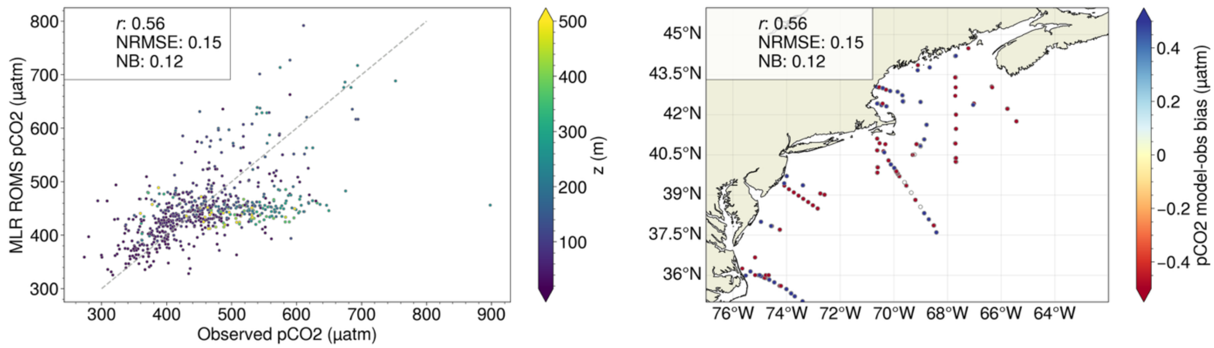

Figure S14: MLR from McGarry et al. (2021) derived pCO_2 comparison between observations and simulations in a scatter plot colored by depth and in a map for bottom waters (right). Model evaluation statistics reported in the inset box of each figure.

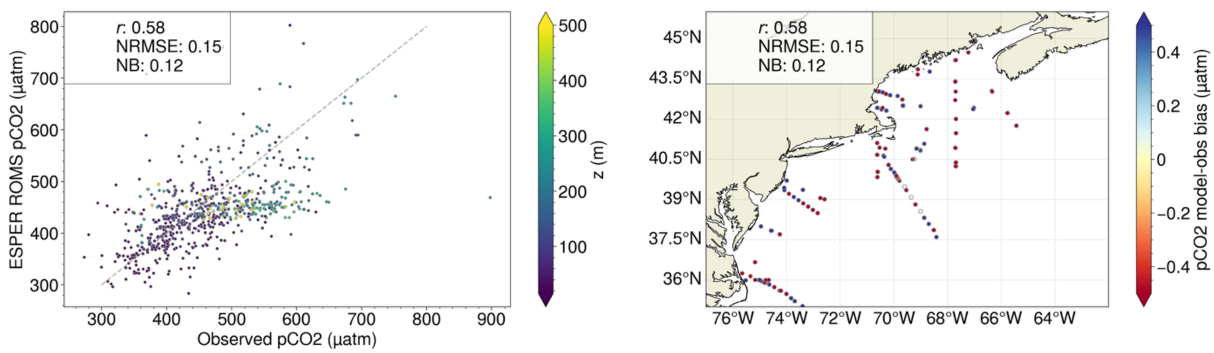

Figure S15: ESPER-NN (Carter et al. 2021) derived pCO_2 comparison between observations and simulations in a scatter plot colored by depth and in a map for bottom waters (right). Model evaluation statistics reported in the inset box of each figure. Observations are retrieved from CODAP-NA from 2007 to 2014.

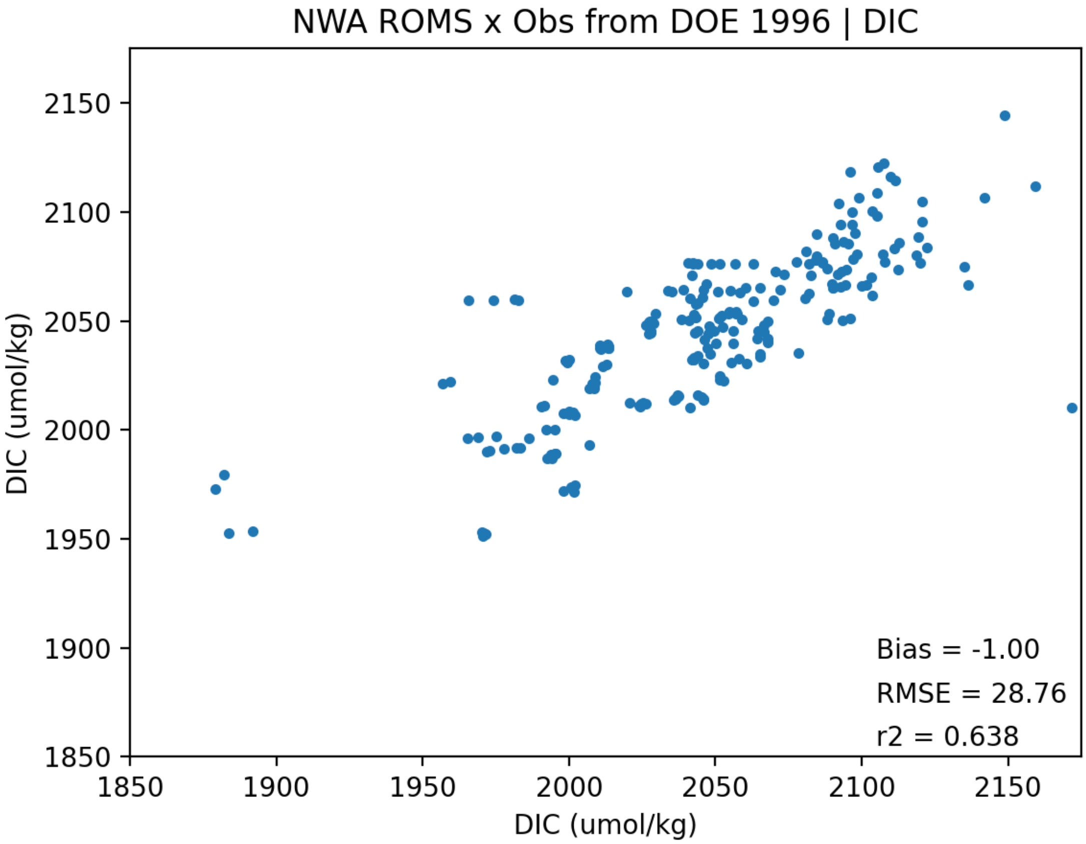

Figure S16: *ESPER-NN (Carter et al. 2021) derived DIC comparison between DOE-OMP EN279 cruise observations and simulations in a scatter plot. Model evaluation statistics are reported in the figure.*

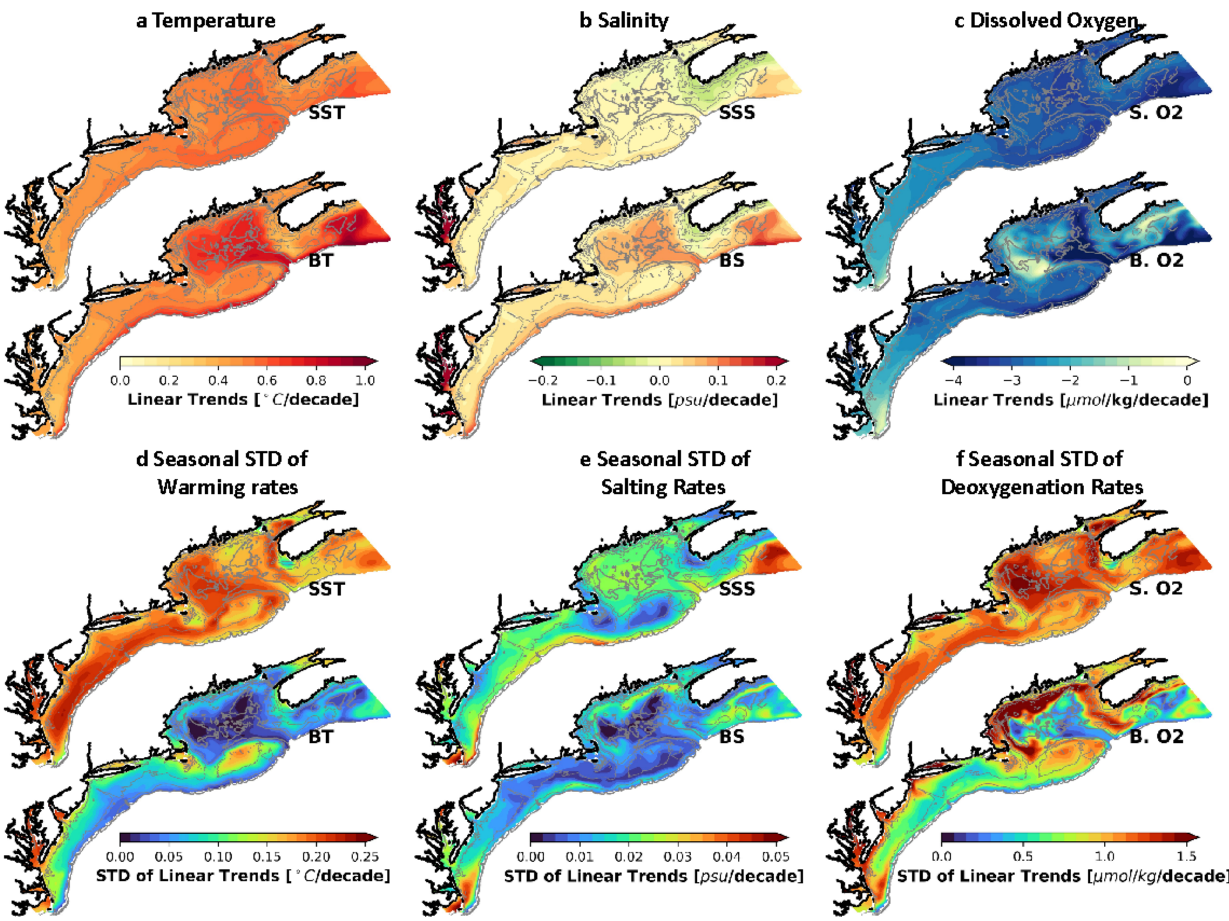

Figure S17. Projected long-term (2015-2098) trends of surface and bottom temperature (**a**; °C decade^{-1}), salinity (**b**; psu decade^{-1}), and dissolved oxygen (**c**; μmol kg^{-1} decade^{-1}) over the NEUS shelf and their corresponding seasonal difference (represented by the standard deviation (STD), **d-f**), based on a dynamically downscaled "time-varying delta" forced ROMS-COBALT-NWA simulations from a global ESM (GFDL) under the SSP5-8.5 emission scenario (see Data and Methods; *Chen et al.*, in prep.).

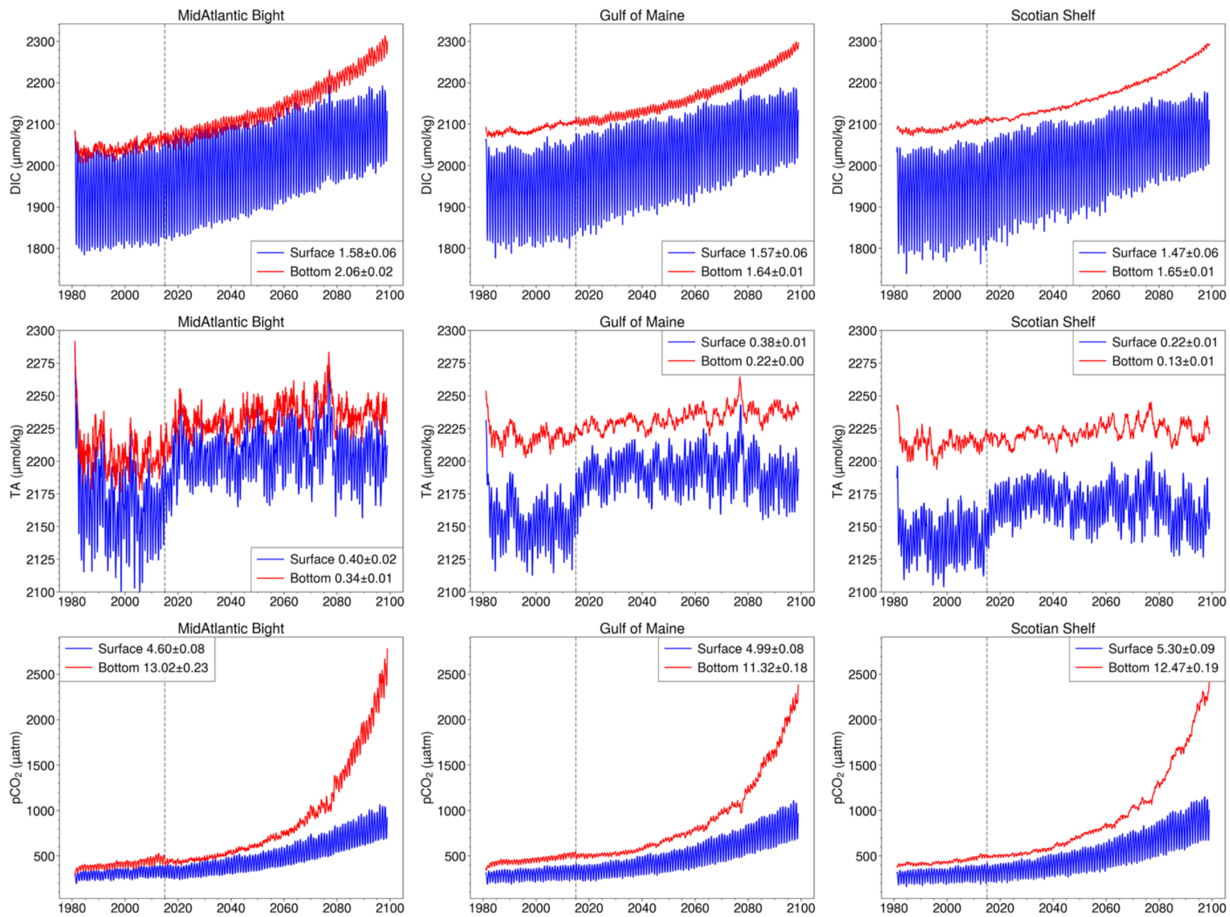

Figure S18: Monthly averaged regional trends from the surface (blue) and bottom (red) spanning the historical simulation (1980-2014, the dashed vertical line) through the future projection under SSP5-8.5 (2015-2098). The top row depicts the trends for DIC the middle row depicts TA, and the bottom row pCO_2. The left column are from the Mid-Atlantic Bight. The middle row are from the Gulf of Maine, and the right column are from the Scotian Shelf. The rates of change (per year) for each time series over the entire record (1980 to 2098) are the values provided in the legend.

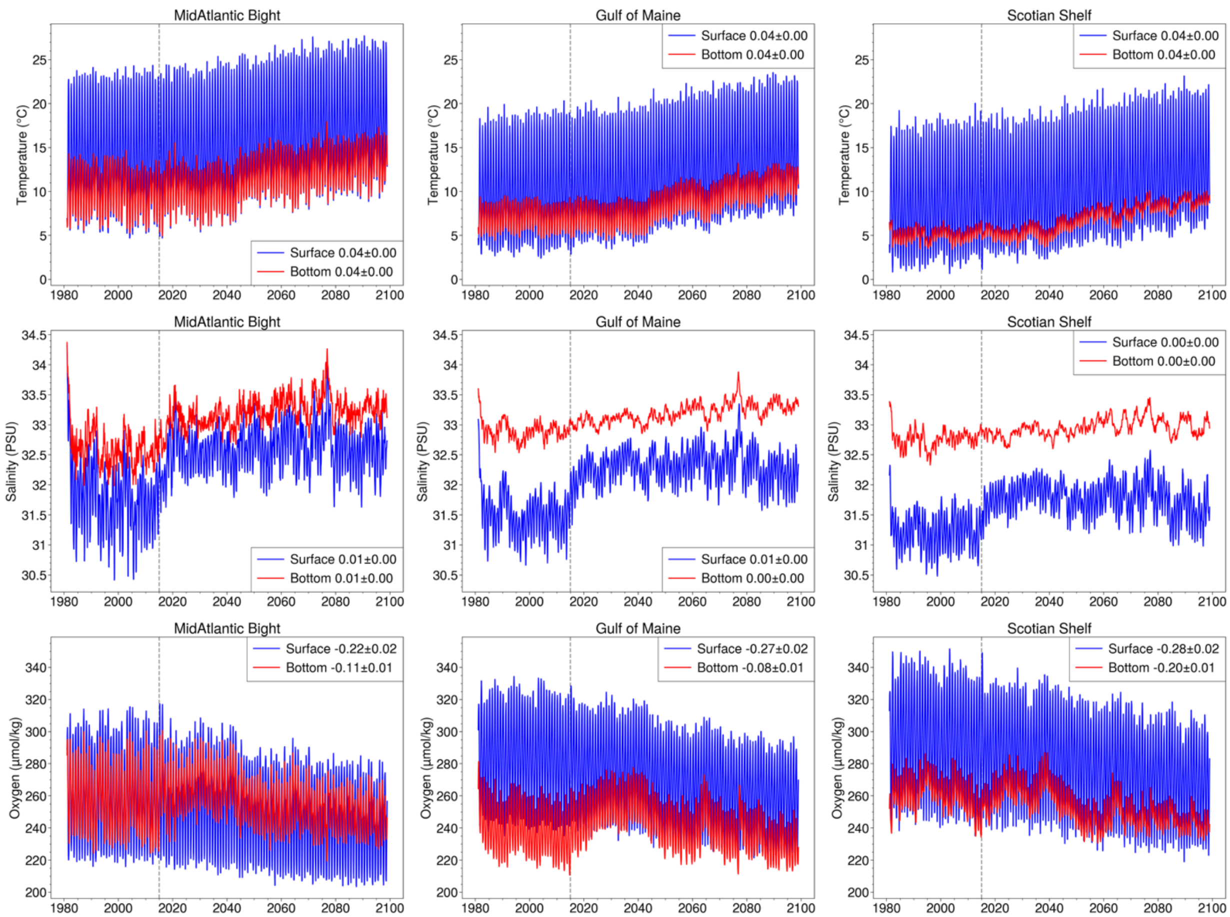

Figure S19: Monthly averaged regional trends from the surface (blue) and bottom (red) spanning the historical simulation (1980-2014, the dashed vertical line) through the future projection under SSP5-8.5 (2015-2098). The top row depicts the trends for temperature, the middle row depicts salinity, and the bottom row oxygen concentrations. The left column are from the Mid-Atlantic Bight. The middle row are from the Gulf of Maine, and the right column are from the Scotian Shelf. The rates of change (per year) for each time series over the entire record (1980 to 2098) are the values provided in the legend.